Sectorized FMCW MIMO Radar by Modular Design With Non-Uniform Sparse Arrays

CRISTIAN A. ALISTARH [1,2] (Graduate Student Member, IEEE), SYMON K. PODILCHAK [1,2] (Member, IEEE),
PASCUAL D. HILARIO RE [1], THOMAS M. STRÖBER[1], YAN PAILHAS[1], CAROLINA MATEO-SEGURA[1],
MATHINI SELLATHURAI [1] (Senior Member, IEEE), GEORGE GOUSSETIS [1] (Senior Member, IEEE),
YVAN R. PETILLOT [1], JOHN S. THOMPSON [2] (Fellow, IEEE), AND JAESUP LEE[3]

(Regular Paper)

[1]Institute of Sensors, Signals and Systems, Heriot-Watt University, EH144AS Edinburgh, U.K.
[2]Institute for Digital Communications, University of Edinburgh, EH93JL Edinburgh, U.K.
[3]Samsung Advanced Institute of Technology, Suwon 443-803, South Korea

CORRESPONDING AUTHOR: Symon K. Podilchak (e-mail: s.podilchak@ed.ac.uk).

ABSTRACT Automotive radars are designed to enhance road user safety and reduce the number of accidents on public roads and there is a constant demand to improve the performance for these radars. In this paper, a novel proof-of-concept multiple-input multiple-output (MIMO) radar architecture is presented by frequency modulated continuous waveform (FMCW) transmission. For enhanced angular resolution, the radar uses a two-tier antenna setup leading to a sparse array arrangement, mainly in an effort to mitigate grating lobes and to offer different illuminations of the same scenario. Also, the experimentally verified sparse radar antenna designed for target detection at the receiver, achieves modest sidelobe levels and grating lobes well below 12 dB from the main beam maximum, whilst still maintaining competitive half-power beamwidths when compared to more conventionally spaced arrays. Moreover, the high impedance bandwidth of this receiver array and the supporting radar electronics (more than 6%) allows for the detection of targets at only a 10 cm spatial separation. The complete system is also capable of seeing a wide field-of-view (FOV) since it utilizes a network of radar modules to cover the forward $-90°$ to $+90°$ angular range by sectorization. In the best case, the measured radar system can resolve targets that are a distance of just $\pm 2°$ apart in angular separation.

INDEX TERMS Automotive radar, antenna systems, array design, millimeter-wave, MIMO, radar antennas, radar subsystem.

I. INTRODUCTION

At the beginning of 2020, autonomous vehicle markets have been globally expanding, with novel technology-ready solutions being investigated in order to make autonomous driving safer and more reliable. Extensive efforts have been made by government and industry to promote intelligent mobility in recent years. According to [1], between 2014 to 2018, ₤120 million has been invested in the United Kingdom for research into connected and autonomous vehicle (CAV) applications.

Moreover, it is estimated that the total global CAV sector will be worth ₤906 billion by 2035 [2].

In order to make autonomous technology a reality, detection of objects and vehicles requires accurate and a real-time response. At the time of writing, self-driving cars still have to fill a technological gap in order to be legally approved for road use, hence many works found in the literature approach the problem of radar resolution [3]–[7]. The discussions focus on both azimuth and range resolution while maximising the
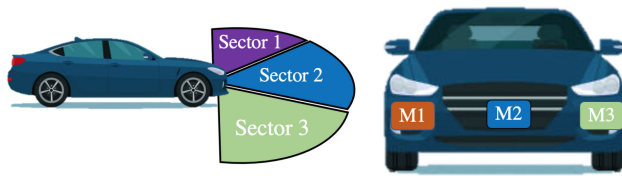
FIGURE 1. Sectorized radar concept using multiple radars across the front bumper of an automobile, where the forward ±90° FOV is sub-divided into three 60° sections or sectors. These multiple RMs for each section are labelled *M*1, *M*2, *M*3 on the bumper (see right).

angular span, also termed as the field-of-view (FOV). These high performance radars are made innovative with techniques including but not limited to beamforming, antenna engineering, target detection algorithms, orthogonal transmission, and clever RF front-end design.

A single radar system with high angular resolution implies a large antenna front-end. Depending on the carrier frequency, car manufacturing requirements and space available on the vehicle, the designer has to restrict the size of the radar front-end to specific dimensions. Our proposed radar architecture for proof-of-concept, which is an extension of the work presented in [8], is to employ repeated radar units for concurrent operation enabling a collective radar system by frequency modulated continuous waveform (FMCW) transmission. The novelty consists of the use of sparse antenna arrays designed through a tiling method proposed in this paper.

This sectorized approach means that the forward (±90°) and complete angular radar spectrum is covered. Basically, the approach illuminates specific sectors of the FOV by assigning multiple radar modules (RMs) to the three 60° sectors (see Fig. 1), which are individually monitored by a sub-radar with 32-elements. These radars, for each sector, also use multiple-input multiple-output (MIMO) virtual array principles to define the effective receivers. This collective system arrangement offers improved functionality and radar performance when compared to the individual RMs, which can only cover a confined FOV, as well as more conventional radar design strategies.

We define our radar antenna system as a sparse array because we are able to reduce the number of elements for the aperture length from 47 elements to only 32 elements, achieving a 32% element reduction. As further described in the paper, these 32 elements monitor a well-defined FOV using multiple RMs. Our approach can also reduce costs due to the scalability and repetition of the required RM hardware and radar antennas. This makes the system maintenance and repair simpler in that individual RMs can be replaced or fixed, rather than the entire radar system itself. This modular or networked design strategy also fosters low-cost mass production of the RMs rather than the assembly and manufacturing of an equivalent non-discrete or non-tiled radar; i.e. a more complete or classic radar system.

By considering the appropriate scheduled signal processing for the individual RMs, all transmission line traces are kept at

a minimum electrical length, reducing losses and noise susceptibility. This would not be possible for an equivalent and more standard (or larger scale) radar architecture. In addition, the monolithic microwave integrated circuits (MMICs) connected to the antenna front-ends can be physically separated (in practice discretely encapsulated for example) to reduce electromagnetic coupling between radar electronics. These design considerations also support easy maintenance of the relevant radar hardware.

The problem of grating lobes and possible false targets are also mitigated in our radar system by the implementation of a MIMO radar receiver made possible by sparse array theory [9]–[11]. Following these works, we define our MIMO sparse array as a radar antenna formed of transmitters and receivers which cooperatively combine several illuminations of the target for a larger effective aperture (or virtual array). Moreover, to study this for the developed radar system, a static $\lambda/2$-spaced receiver was designed for the RMs using substrate integrated waveguide (SIW) technology. Then, the required channels connected to the antenna elements were appropriately selected. In particular, during the radar signal processing of the simulated and measured system, the antenna elements (and the corresponding RF channels) that contribute to the grating lobes were suppressed and mitigated. It is shown in the paper that the overall radar system performance can benefit from this MIMO sparse array approach whilst preserving a large antenna aperture for the equivalent virtual receiver array. Comparisons are also made in the paper for the radar system response when considering more conventional $\lambda/2$-spaced and λ-spaced radar receivers.

It should be made clear that the inter-element spacing for the receiver SIW antennas plays an important role in the effective virtual antenna aperture for the radar as well as the accuracy in the radar response. This is because grating lobes hinder the performance of the radar by generating false targets when the receiver inter-element spacing is equally spaced at a distance greater than half of a wavelength. To solve this problem, the aforementioned non-uniform spacing at the SIW receiver is introduced and combined with MIMO time domain transmission to obtain a clear angular target estimation for the forward FOV.

This is made possible by installing a network of multiple RMs at different angles on the vehicle bumper considering the adopted scenario for automotive applications (see Fig. 1). Moreover, by employing this sparse array method whilst using a fixed inter-element spacing in multiples of half-wavelengths, due the developed SIW antenna design, the element (and RF channel) selection which dictates the receiver array pattern can be made less complex. This is because the total possible number of arrangements for the array is significantly reduced when compared to a more standard sparse array which might have non-uniform spacing. Similar conclusions were observed in [9] which uses a three transmitter, four receiver antenna configuration.

It should be mentioned that better radar system performance is possible if the receiver spacing is not limited

TABLE 1. Comparison of State-of-the-Art Radar Systems (Measurements) as Reported in the Literature

Radar	Carrier Frequency	Target Estimate Algorithm	Antenna Type	Equivalent Uniform Linear Array	Array Element Spacing	Receiver Percentage Bandwidth	Range Resolution	FOV[1]	Θ_{3dB}	Time (ms)	SLL (dB)[2]
[3]	76.5-77 GHz	Analog Beamforming	Microstrip Arrays	32	0.6λ	5.2% (4 GHz)	3.75 cm	$\pm50°$	5.5° to 7.0°	100	-15
[12]	120 GHz	MIMO Digital Beamforming	Circular Patch Antennas	16 (= 2×8)	Sparse Non-uniform	4.1% (5 GHz)	3 cm	30°	8.5°	100	-8
[13]	61 GHz	Digital Beamforming	Scalable TRX MIMO radar	4 (= 2×2)	2λ	8.2% (5 GHz)	3 cm	$\pm15°$	6°	-	-11.8
[6]	75-77 GHz	MIMO Digital Beamforming	Differential Microstrip Arrays	16 (= 4 TRX modules)	Non-uniform	2.6% (2 GHz)	7.5 cm	$\pm81°$	$3.7 - 6.8°$	-	-13
[14]	79 GHz	MIMO Digital Beamforming	Planar SIW Antenna Arrays	8 (= 2 × 4)	1.75λ	1.2% (1 GHz)	15 cm	$\pm30°$	7°	-	-20
[15], [16]	79 GHz / 150 GHz / 300 GHz	DBS / SAR	Horn Antennas	2 RX	-	6.3% / 3.33% / 1.67% (5 GHz)	3 cm	$\pm40°$	1.2° at v = 0.25 m/s	-	-12
This work	24 GHz	MIMO Digital Beamforming with Sectorization	Planar SIW Antenna Arrays	32 (= 4 ×2 × 4)	Sparse Non-uniform	6.25% / 1.5 GHz	10 cm	$\pm\mathbf{90°}$	4.4° (Tier 1)[3] **2.2°** (Tier 2)[4]	**30**	-8 [5]

[1] Measured field-of-view (FOV),
[2] side-lobe-level (SLL) for the complete radar system,
[3] uniform array configuration,
[4] non-uniform sparse array configuration, and
[5] observed worst case (as will be further described in the paper, measured values range from −8 dB to −13 dB).

to multiples of half-wavelengths, hence some methods of discovering these positions can be carried out with simulated annealing as in [9]. However, the method applied in our paper has the advantage of finding the approximate solution by following a heuristic approach, which conforms with the largest aperture size possible for the virtual array whilst not degrading radar system performance. As further discussed in the paper, our methodology also supports a two-tier or dual-mode detection scheme using a network of RMs for specific FOVs. The first detection is carried out considering $\lambda/2$- or λ-spaced receivers, and then, secondly, reconfigured for more accurate detection considering a sparse or non-uniformly spaced array. Then the angular target estimation response is computed from the relevant receivers considering the achieved MIMO virtual array.

The paper is organized as follows. Sections II discusses the state-of-the-art for automotive radar while Section III

presents the mechanisms of FMCW radar, its general structure and our proposed architecture. Section IV outlines the developed millimeter-wave radar system. Section V discusses the performance of the transmit and receive SIW antennas for the radars. Section VI presents the experimental setup for the radar, and the results of the measurement data. Section VII concludes the findings of this paper.

II. STATE OF THE ART AND RADAR DESIGN MOTIVATIONS

A number of other radar solutions have been reported in literature for high angular resolution and are summarized in Table 1. The work presented in [3] used analog beamforming with 2 transmitter and 16 receiver elements (vertically polarised) defining the radar antenna front-end. While a range resolution of 2.5 cm was achieved with a 5.2% impedance matching bandwidth and minimal beam squinting, the FOV only covers $\pm50°$. The half-power beamwidth (Θ_{3dB}) ranges

between 5.5° to 7°. In [12], a 120 GHz compact radar system was presented to show that it is possible to employ integrated circular antennas to achieve a high range resolution, whilst adopting a 5 GHz radar bandwidth. Furthermore, in [13], it was shown possible that different transmit-receive (TRX) architectural blocks can be configured and spaced appropriately to achieve better target detection when compared to more conventional MIMO strategies.

The work presented in [4] used quasi-optical elements to form a large aperture which produced a Θ_{3dB} of 4° with only 4 quartz glass resonator antennas. However, the FOV covered was only ±30°, a configuration suitable for long-range radars (LRRs). An ultra-wide band short-range radar (SRR) sensor was presented in [14] for operation at 79 GHz. That radar was configured using substrate-integrated waveguide (SIW) antennas allowing for increased gain, broad FOV and narrow beams. Also, by using a combination of pulse compression methods and digital beamforming, the radar was able to detect objects up to 90 m, with a range resolution of 10 cm, a FOV of ±35°, and an angular target resolution of 7°. Recently, works have also been carried out in the low-terahertz frequency range. This is because research has shown that absorption losses between 100 GHz and 900 GHz does not exceed 3 dB/km, hence detection ranges up to 200 m are achievable [17]. For example, high resolution images have been obtained with a 1.2° angular resolution (see [15], [16]) where increased frequencies allowed for larger bandwidths and thus improved range resolution. In addition, novel processing techniques such as Doppler beam shaping (DBS) have been adopted from aerospace engineering principles for advanced imaging techniques [15].

To compliment and advance these findings our newly proposed radar system in this paper uses SIW antennas with non-uniform element spacing which further develops our preliminary results as presented in [8]. This antenna selection and its distinctive features, along with the radar electronics which offer high bandwidth, provides significant benefits as compared to other radars (see Table 1) in terms of FOV, the angular resolution (i.e. Θ_{3dB}) for the radar, and the detection time. More specifically, we develop and examine in this paper a 24 GHz radar system prototype using three different sectors to divide the complete FOV (also defined herein as a sectorized radar) as illustrated in Fig. 1 for automotive applications (for example), but can also be applied to other scenarios. The system is capable of refined angular resolution due to the developed two-tier detection procedure by considering sparse arrays to achieve better angular resolution, and multiple radar modules (RMs) for a larger effective FOV. Also, the use of the designed SIW antennas offers a broad impedance matching bandwidth to achieve high range resolution. Using these multiple RMs to monitor the FOV, the system architecture allows for several sectors to be illuminated to obtain a ±90° image while also achieving an angular resolution of 2.2° and a range resolution of 10 cm.

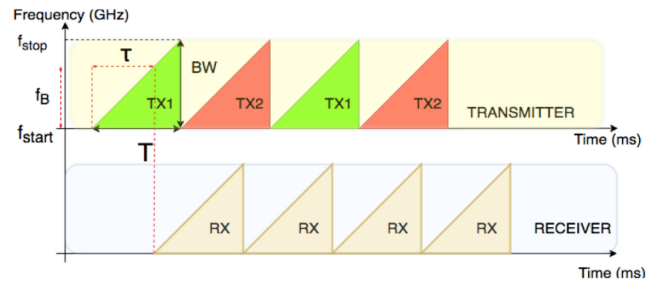The 24 GHz frequency band was chosen because the radar hardware as well as the supporting MMICs are commercially

FIGURE 2. Frequency modulated continuous wave (FMCW) transmission showing a two transmitter MIMO antenna system with time domain multiple access.

available. This offers simple integration, low-cost implementation for research and development, and proof-of-concept demonstration for our proposed radar system architecture. More specifically, the ultra-wide band (UWB) range for automotive radars have been used in this work for testing the proof-of-concept demonstrator. The allocation of the 24 GHz ISM and UWB frequency bands are explained further in [18] and [19]. It should also be mentioned that a scaled-down version of the radar system, for operation at 77 GHz for example (or other microwave and millimetre-wave frequencies), is possible and can define future work. However, the motivation of the present research is development and study of the proposed MIMO radar system architecture using multiple RMs whilst employing sparse antenna arrays for enhanced angular resolution.

There are several challenges at 77 GHz as mentioned in [20] and [21]. Firstly, 77 GHz radars are smaller in size and packaging is very important at these frequencies since it can significantly contribute to the losses of the radar system. This is a performance penalty that needs to be considered during the radar design and hardware manufacturing. For example, some of the possible on-chip losses are described in [21] whilst considering several antenna-on-chip technologies. Another disadvantage for working at 77 GHz is the increased cost for the antenna manufacturing due to the required tolerances. This is because the size of an antenna design at 77 GHz is about three times smaller than one at 24 GHz whilst considering the wavelength. Lastly, these practical manufacturing tolerances may cause some inaccuracies, and it is possible that the actual antenna performance might be slightly different from its expected parameters which can degrade the radar system. For these reasons, the reported antenna and radar system was designed at 24 GHz, mainly, for proof-of-concept of the proposed radar system architecture.

III. FMCW RADAR SYSTEM PRINCIPLES
A. FMCW RADAR RANGING CONCEPTS
Frequency modulated continuous wave (FMCW) radars make use of chirps to identify targets located at a distance by analysis of the frequency difference between the transmitted and received signals (see Fig. 2). By down-mixing the transmitted and received signal, the resultant intermediate frequency

(IF) signal has the information of both range and speed of the target. This process is called target acquisition and range tracking [22].

The linear modulated waveform or a linear chirp is a signal which has a linear variation in frequency. To better understand the concept, a sinusoidal signal is taken [23]:

$$x(t) = A \sin(\phi(t)) \tag{1}$$

where A is the amplitude and $\phi(t)$ is the signal phase. The derivative of the phase is the instantaneous angular frequency [24]:

$$w(t) = \frac{d\phi(t)}{dt}, \quad w(t) = 2\pi f(t) \tag{2}$$

$$f(t) = \frac{1}{2\pi} \times \frac{d\phi(t)}{dt}; \tag{3}$$

The frequency rate or chirp rate is defined by the rate of change of the frequency [24]:

$$c = \frac{1}{2\pi} \times \frac{d^2\phi(t)}{dt^2} = \frac{df(t))}{dt}; \tag{4}$$

Since it is known that a linear frequency modulated signal has a linear frequency response over time [23], we can write that signal as:

$$f(t) = f_0 + kt \tag{5}$$

where f_0 is the starting frequency, k is the slope of the chirp and t is the time variable. Also, k is defined as:

$$k = \frac{f_1 - f_0}{T} \tag{6}$$

where f_1 is the stop frequency and T is the period to sweep between f_0 and f_1. Since the frequency behaves linearly within the sweep, one is able to compute the phase of the chirp by taking the time integral of the frequency.

$$\phi(t) = \phi_0 + 2\pi \int_0^\tau f(\tau)\, d\tau$$
$$= \phi_0 + 2\pi \int_0^\tau (f_0 + k\tau)\, d\tau$$
$$= \phi_0 + 2\pi \left(f_0\, t + \frac{k}{2}\tau^2\right) \tag{7}$$

where the linear modulated waveform signal (or linear chirp) can be written as [23], [24]:

$$x(t) = \sin\left[\phi_0 + 2\pi \left(f_0\, t + \frac{k}{2}\tau^2\right)\right]; \tag{8}$$

Usually, the initial phase at $t = 0$ is zero. The chirp is therefore a frequency modulated (FM) signal which has a linear change of rate in the frequency domain.

B. ANGULAR TARGET LOCALISATION

The beamforming method, also called delay and sum (DAS) has been adopted in this paper as the main beamformer since it is a fast and simple method for target detection [25]. However, DAS has coarse angular resolution compared to adaptive
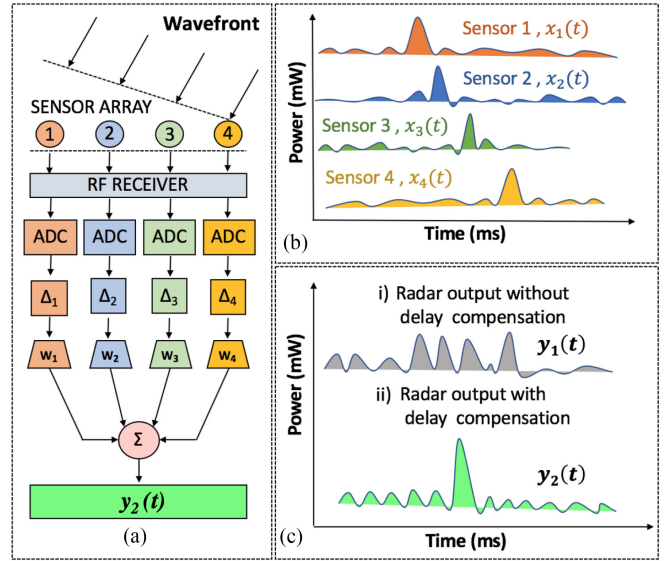

FIGURE 3. Receiver digital beamforming: (a) structure, (b) time domain signals, (c) radar beamforming returns without and with delay compensation caused by antenna inter-element separation.

beamforming methods or compressed sensing [25]. A complete review of automotive radar signal processing and beamforming methods such as MUSIC, MVDR and Compressive Sensing can be found in [26]–[29].

The process of narrowband beamforming consists of adding delays and weights to each of the receiver paths and is depicted in Fig. 3(a). The individual time domain signals at each RX antenna sensor, $x_i(t)$, can be observed in Fig. 3(b). After the collected time domain signals are sampled, they are then time shifted by a delay δ_i and weighting w_i according to the contribution of each sensor element. If the signals of each sensor are not delayed according to their position, the output of the beamformer can be determined according to the expression:

$$y_1(t) = \sum_{i=1}^N w_i x_i(t) . \tag{9}$$

This result does not maximise the true position of the target [30] (see Fig. 3(c)). On the other hand, if the time delays δ_i due to antenna element spacing are considered, the output sum indicates the highest power received for that particular angle according to the expression [22]:

$$y_2(t) = \sum_{i=1}^N w_i x_i(t) e^{-j\omega\Delta_i} \tag{10}$$

Once this has been carried out, the resultant signals are measured at each scanning angle to combine the returns measured in the directions of interest.

The unambiguous FOV is defined as the angular space in which the radar is able to detect a target. For a radar system

this parameter is defined as [31]:

$$\Theta_{FOV} = \pm \sin^{-1}\left(\frac{\lambda}{2\,d}\right) \qquad (11)$$

where λ is the wavelength and d is the uniform inter-element spacing of the receiver antenna elements. A widely accepted definition for radar angular resolution is not yet present in the literature [4], [32], however, there is a wide acceptance of the Rayleigh criterion metric. Here it is defined for both uniformly and non-uniformly spaced receiver arrays:

$$\Theta_{3\,\mathrm{dB}} = \frac{180°}{\pi} 1.22 \frac{\lambda}{d_1 + d_2 + \cdots + d_N} \qquad (12)$$

where $d_1, d_2 \ldots, d_N$ are the distances between each of the elements. The sum of all these distances equals the effective aperture of the receiver array.

C. SIMO & MIMO RADAR SYSTEMS

Single-input multiple-output (SIMO) radars are conventional radar configurations which have one transmitter and usually equally spaced receivers defined as a uniform linear array (ULA). Multiple-input multiple-output (MIMO) radars, on the other hand, can provide increased angular resolution for automotive detection systems because these radars can emulate an increased aperture size for the receiver antenna array [26]. MIMO systems also combine the advantage of using multiple reflections from transmit/receive paths. The targets are illuminated successively from different views, taking into account the positioning of the antenna sensors [29].

MIMO antennas also bring more spatial diversity. Emerging antenna designs provide beamsteering which can improve radar resolution in addition to the transmitted power distribution [33]. MIMO systems have also seen a proliferation among radars designed for automotive applications [34]–[36]. This is especially true due to the well-known principles behind MIMO processing which have been adapted from digital communication systems [33], [37], [38]. The advantage of using MIMO radar front-ends is also related to the increased illumination of the target for a defined FOV. At the same time, MIMO systems use spatial antenna distribution to increase the virtual aperture length by convolving the antenna signals. Furthermore, signal orthogonality is key to multi-antenna transmission systems, especially when concurrent transmission is taking place. The received signal strengths vary for different radar cross sections (RCS) of the targets, however increased aperture length and illumination from different positions makes target identification easier.

According to the MIMO theory described in [9], the positions of the N_{TX} transmitters, together with the positions of the M_{RX} receivers constitute an equivalent array, also termed the virtual array. The following steering vectors can be defined for this virtual array:

$$\mathbf{y}(\phi) = e^{i\frac{2\pi}{\lambda}(d^{Tx} \bigoplus d^{Rx})u}, \qquad (13)$$

where d^{Tx}, d^{Rx} are the transmitter and receiver antenna element positions, and $d^{Tx} \bigoplus d^{Rx}$ ($= d_1^{Tx} + d_1^{Rx}, d_1^{Tx} + d_2^{Rx}, \ldots., d_N^{Tx} + d_M^{Rx}$) represents the antenna virtual array configuration based on the convolution of the transmitter and receiver antenna element positions. The aperture of this equivalent virtual array has a total number of $N_{TX} \times M_{RX}$ element positions. The advantage of using this MIMO configuration is the reduced sensor footprint and RF hardware requirement when compared to an equivalent uniform linear array of the same size. In general, it is expected that for an array of size $N_{TX} \times M_{RX}$ antenna sensors, the total physical area is reduced to only $N_{TX} + M_{RX}$ antenna sensors for the radar front-end.

D. MILLIMETRE-WAVE RADAR CONFIGURATIONS
In order to assess the benefit of using several modules together, the radar configurations have been simulated in MATLAB. The trialled radars and their configurations are illustrated in Fig. 4 .

1) SINGLE-INPUT SINGLE OUTPUT (SISO) RADAR (FIG. 4(A))
This refers to the single transmit single receive radar configuration.

2) RADAR MODULE (FIG. 4(B))
This configuration is defined by two transmitters and four receivers defining an elementary MIMO radar module (RM).

3) MODULAR MIMO RADAR (FIG. 4(C))
This radar configuration uses a combination of four MIMO sub-modules; i.e. four distinct RMs where each RM is defined by two transmitters and four receivers. This defines the modular MIMO radar system to have 32 ($= 4 \times 2 \times 4$) virtual receiver antenna elements.

4) SECTORIZED MIMO RADAR FRONT-END (FIG. 4(D))
The final configuration is composed of three modular MIMO radars which are assigned in three sectors to cover the range from $-90°$ to $+90°$. Each sector is operating in the time domain with multiple access i.e. TDMA, to reduce inference between radars. An overview of signal processing schedule for the radar can be seen in Fig. 6. Other MIMO works, which do not consider sectorization, solve the problem of concurrent transmission using orthogonal frequency division multiplexing (OFDM) (see [39]–[41]).

When trying to determine the sensitivity of the sectorized radar system, it is useful to quantitatively compare the range detection capability of all configurations (see Fig. 4) with respect to the signal-to-noise ratio (SNR). By assuming that the modules are similar in configuration (with respect to the gains of the antennas and placement), the SNR of the sectorized radar case has a direct dependence on distances from the transmitters and receivers to each target.

A simulation in MATLAB has been developed to match configurations in Fig. 4 and to test the SNR performance with the radar equation. The results of the simulation are presented
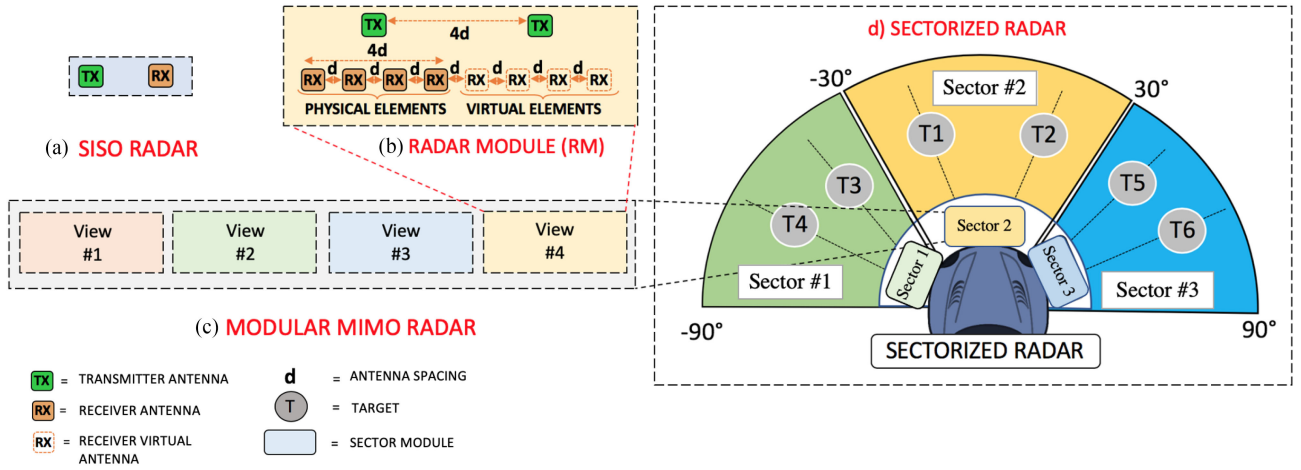
FIGURE 4. Proposed automotive radar and antenna configuration: (a) SISO, (b) a MIMO radar module (RM) defined by 2 physical transmitters (TX) and four receivers (RX), (c) modular MIMO radar system defined by 32 antenna elements in total (= 4 RM × 2 TX × 4 RX) for each sector, and, (d) the complete sectorized MIMO radar system covering the complete ±90° FOV. Here also 6 targets are illustrated in (d) for each sector.
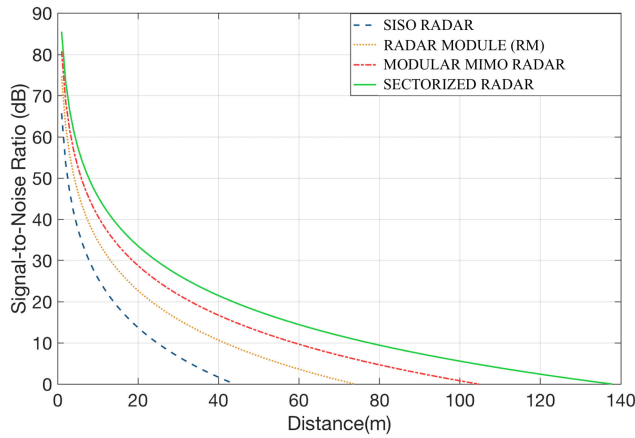

FIGURE 5. SNR simulations of the radar configurations: SISO radar (1TX/1RX), MIMO RM (2TX/4RX), modular MIMO radar (8TX/16RX) and sectorized radar (24TX/48RX).
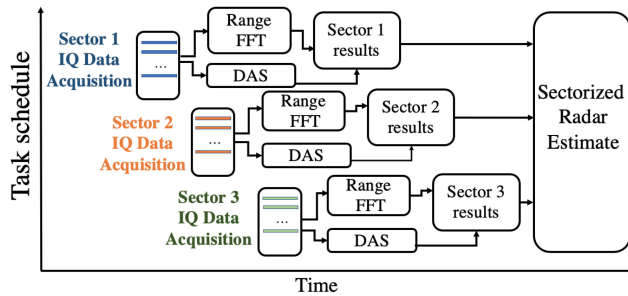

FIGURE 6. Workflow diagram for the signal processing of the sectorized radar for one acquisition cycle.

in Fig. 5. The SNR was calculated according to [22]:

$$SNR = \frac{P_T \ \tau \ G_T G_R \lambda^2 \sigma}{(4\pi)^3 k T_s R_T^2 R_R^2 L} \quad (14)$$

where P_T is the transmitted power (8 dBm), τ is the pulse period (50 ms), G_T and G_R are the transmitted

and received gains (22 dB for each), λ is the wavelength (1.25 cm), σ is the RCS (defined by a square metallic target of size 20 cm by 20 cm), k is the Boltzmann constant (1.38 × 10^{-23} $m^2 \ kgs^{-2}K^{-1}$), T_s is the system temperature (at 25°C), R_T and R_R are the transmitted and received ranges while L is the path loss at 24 GHz (−86 dB).

For the RM case, doubling the number of transmitters and four-folding the number of receivers (Fig. 4(b)) should theoretically result in improvement of eight times the SISO gain. Also, a minimum 1.5-fold improvement can be observed in simulations when doubling the number of elements at the receiver beamformer. With some further study and the re-arranging of (14) and whilst taking the ratio between the range of the sectorized radar (R_S) and the SISO radar (R_M), the following equation can be obtained:

$$\left(\frac{R_S}{R_M}\right)^{1/4} = \frac{G_S/P_S}{G_M/P_M} \quad (15)$$

where G_S and G_M are the gains of the sectorized and SISO radars while P_S and P_M are the received powers for the two configurations. The gains and the sensitivity of the radars directly affect their performance. Hence the gain improvements compared to the SISO case for the configurations presented in Fig. 5 are: 5.28 dB (Fig. 4(b)), 8.82 dB (Fig. 4(c)), 13.57 dB (Fig. 4(d)). As seen in Fig. 5, the detected range is more than doubled by the sectorized radar compared to the SISO case due to the gain improvement. When comparing the green and black curves the difference is 4 dB, which corresponds to (8). While the modular MIMO radar exhibits a further four-fold SNR improvement compared to the basic MIMO radar. Also, the sectorized radar increases the SNR of the modular MIMO case by three due to the number of sectors.

E. GENERAL DISCUSSIONS

The proposed sectorized radar configuration is able to detect on average with twice the sensitivity of a modular MIMO
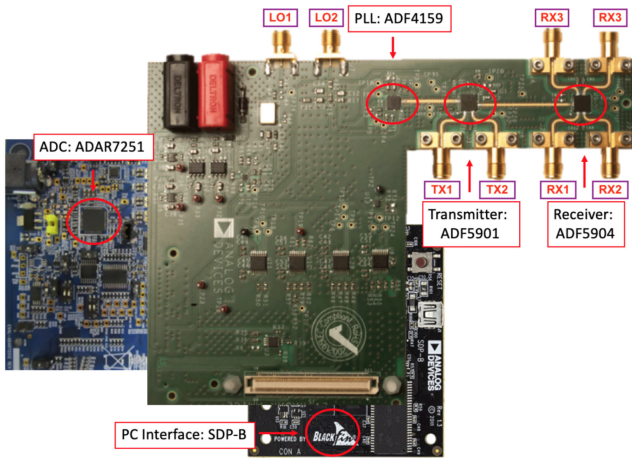
FIGURE 7. Photograph of the 2TX by 4RX radar electronics defining an individual RM.

FIGURE 8. Radar connection and signal processing diagram for a single RM.

FIGURE 9. TX and RX block diagram for an individual RM.

TABLE 2. Circuit Components for the Radar

Circuit Component	Supplier	Part Number
Phased Lock Loop	Analog Devices	ADF4159
Transmitter MMIC (2TX)	Analog Devices	ADF5901
Receiver MMIC (4RX)	Analog Devices	ADF5904
Low Noise Amplifier	Hittite	HMC751LC4
MESFET Switch	Hittite	HMC1084LC4

radar configuration because of the increased number of elements, which adds gain to the overall radar link budget, allowing for more detection range. To achieve better angular resolution, a larger antenna aperture must be designed and this can be achieved using element spacings of λ instead of the conventional $\lambda/2$ for the radar receiver antenna. However, this is at the cost of a reduced FOV due to the presence of grating lobes (for the λ-spaced array which defines a FOV of $60°$) and this is why three sectors are employed for each radar as illustrated in Fig. 4(d). This defines Tier 1 detection (see Table 1). Another radar antenna design can be considered which is the optimal element spacing with array sparsity for the array which can help to control side-lobe levels (SLLs), mitigate grating lobes, and improve angular resolution. This array sparsity approach defines possible detection for Tier 2 (see Table 1). These topics are discussed further in the next few sections.

IV. DEVELOPED MILLIMETRE-WAVE RADAR SYSTEM

The preliminary MIMO radar developed by the authors in [8] used two transmitting antennas (2TX) and four receiver antenna elements (4RX). This initially developed MIMO radar configuration is now used as a building block in the following for developing the proposed two mode radar system with FOV sectorization. Also, the antenna transceivers work in a time domain sequence; i.e. TDMA, in order to avoid signal interference while maintaining orthogonality. The process of acquiring a sectorized radar estimate is shown in Fig. 6. A photo of the radar system hardware and the radar block diagram can be seen in Figs. 7 and 8, respectively. Also, the circuit-system architecture for an individual MIMO RM is outlined in Fig. 9.

The radar system uses monolithic microwave integrated circuit (MMIC) components from Analog Devices and Hittite (a summary is presented in Table 2). Signals are generated at the transmitter (model: ADF5901) by using a calibrated voltage controlled oscillator (VCO) preceded by a varying ramp signal generated by a phased lock loop (PLL) (model:
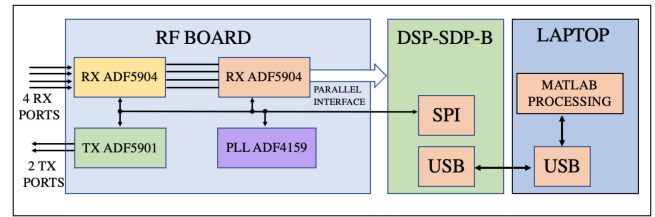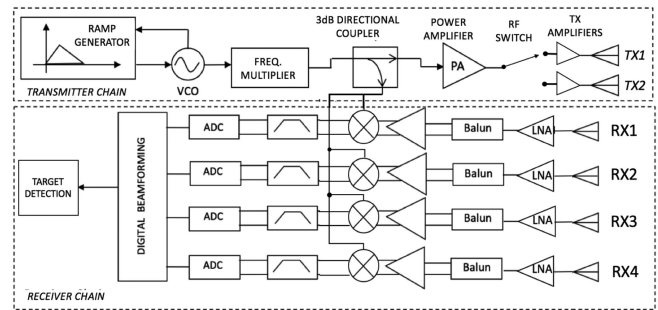
ADF4159). This allows for the signal to operate in FMCW transmission. Also, the signal obtained at the output of the VCO is then up-converted to 24 GHz. The ADF5901 has an internal amplifier to reach an output power up to +8 dBm. In addition, the transmitter antennas are used in the time domain with multiple access (i.e. TDMA) since the ADF5901 has an RF switch that can alternate the use of the transmitters by using a Hittite HMC1084LC4 switch (one for each RF channel).

The receiver is also connected to a 24 GHz VCO which is part of the down-converter. Including a low noise amplifier (LNA) (Hittite HMC751LC4) in cascade at the receiver input also lowers the noise level according to Friis's formula [42]. After the signal is down-converted, it passes through a band-pass filter in order to remove unwanted higher order modulation products generated by the mixer. The signal is then sampled by an analog-to-digital converter (ADC) and passed to the digital beamforming network. Differential lines are used

TABLE 3. Three Different RM Transmitter Outputs

Sector	Power Mean (dBm)	Average Power Deviation (dB)	Phase Error (deg)	Frequency Error (kHz)	Slope Frequency Error (kHz)	Bandwidth per Time Period (MHz/μs)	Impedance Matching Bandwidth(%)
1	5.01	0.52	3.59	17.18	72.41	480	6.25
2	4.95	0.53	2.97	14.17	72.21	480	6.25
3	4.82	0.55	4.12	17.17	68.37	480	6.25

Note: See the photos in Fig. 7 and 20(b) for an individual RM and three RMs clustered for system measurements, respectively.
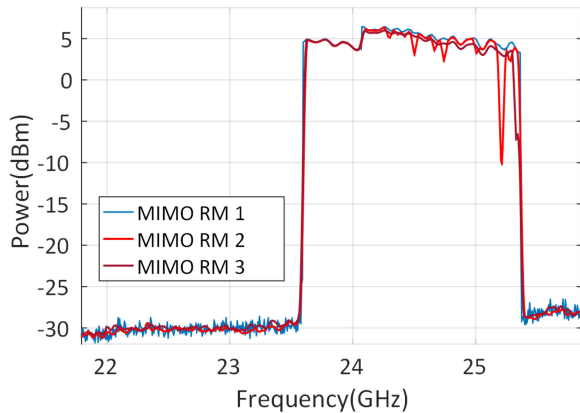

FIGURE 10. Measured transmitter spectrum response for three different 2TX by 4RX MIMO RMs (see Fig. 7) by sampling TX port 1 only. A BW for the transmitter spectrum of about 1.5 GHz is observed, and it is this hardware metric that limits operation of the radar system.

to improve the common mode rejection ratio of the amplifier and reduce noise.

Preliminary findings reported in [8] suggested that by increasing the physical and virtual aperture size of the receiver front-end, improved angular resolution for the MIMO radar system can be made possible. Consequently, it is conceivable that multiple MIMO RMs could be appropriately placed to collaborate, and therefore, be able to achieve better system performance in terms of resolution and target detection when compared to an individual MIMO RM. This design motivation follows the MIMO radar work in [43] which also employs highly separated antennas. However, it is important at this stage to validate that the individual MIMO RMs (see Fig. 4(b)) first detect the targets individually, before integrating them further into a larger radar with multiple RMs. The following sub-sections investigate the sensitivity of detection for different radars starting from the fundamental mono-static radar, and then, leading to the proposed sectorized radar system (Fig. 4(d)) which uses a network of MIMO-RMs.

A summary of the measured linearity parameters for three radar sectors for three different RMs, representative of the three sectors, see Fig. 4(d) are also reported in Table 3 while output power spectrums are shown in Fig. 10. Measurements have been completed using a N9030B PXA Signal Analyzer from Keysight Technologies. The signal bandwidth which could be analysed for the linearity parameters was limited to 50 MHz due to the inner circuit constraints of the PXA analyzer hardware.

In comparison with the results presented in [44] which uses direct digital synthesis (DDS), the transmitter presented in our paper uses a fractional-N frequency synthesizer capable of generating 2 GHz of bandwidth. However, the device can transmit a signal using 13 GHz of bandwidth when triggered by an external source. Clear advantages have been further explained in [45], while both PLLs and DDS can be tailored for certain applications. However, PLLs can be more cost efficient than DDS [45]. This defines a clear advantage when employing such modular radar systems for automotive applications.

As further explained in [46], the ADF4159 PLL uses a 25-bit fixed modulus which allows for sub-hertz resolution at 3μHz for a phase detector frequency of 110 MHz. In addition, a 12 b DAC powers the VCO and the average power consumption of the ADF4159 module is 100 mW. Also, the spurious-free dynamic range (SFDR) for the VCO can reach -90 dBc [46], while the frequency update time per step is 100 ns. The FFT gain of the system is 33 dB. Except for the update time, the fractional-N frequency synthesizer, employed here, shows improved figures of merit for generating the transmitting signal, in comparison to the DDS solution outlined in [44].

V. FRONT END ANTENNA DESIGN

Microstrip antenna arrays have seen a widespread use for automotive radar systems since this type of antenna is simple to design and is easy to manufacture [47]. On the other hand, the radiation losses of substrate-integrated waveguide (SIW) antennas are significantly reduced for millimetre-wave frequencies when compared with microstrip patch antennas as described in [48] and [49]. Also, SIW-type antenna arrays generally are less dispersive when compared to series-fed microstrip structures and other patch-type arrays [50], leading to reduced beam-squint over frequency which is generally desired for improved radar accuracy. A review of SIW technology can be found in [50] while a detailed report of other automotive antenna types was reported in [51].

Following these previous efforts, SIW antennas have been selected for our radar (see Fig. 11). This is because when considering more conventional microstrip patch antennas, the beam can be squinted depending on the transmission frequency; i.e. the main beam position can undesirably change with frequency. This is due to the fixed distance of the radiating elements with respective to the wavelength [52]. More specifically, since the transmission frequency is constantly being changed in an FMCW radar, the beam angle can vary due
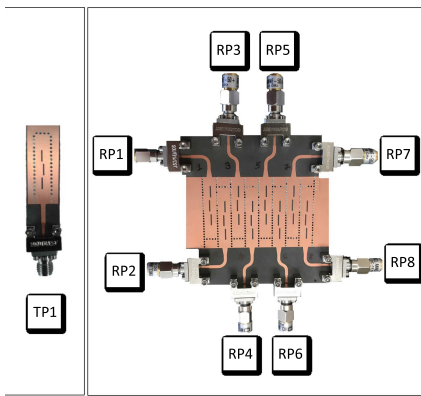
FIGURE 11. Single element SIW TX (left) and 8-element RX (right). The TX and RX SIW antenna ports, are labeled as TP*i* and RP*i*, respectively.

FIGURE 12. Realised gain beam pattern of the SIW transmitter antenna in the horizontal plane.

FIGURE 13. Comparison of theoretical results, simulations and measurements for the $\lambda/2$ array with 4 RX elements using RP3, RP4, RP5, and RP6 (see Fig. 11).

to this dispersion, when employing more standard microstrip-based antenna arrays. A property which is undesirable in radar detection [8].

SIW structures on the other hand support fundamental and dominant TE_{01}-like mode excitation. This mode is generally known to have lower dispersion when compared to the quasi-TEM mode of microstrip [50], [53]. SIW slot-based antennas can also offer reduced (unwanted) beam squint over frequency and can also exhibit reduced electromagnetic coupling because of reduced surface wave losses [50]. Regardless of these features, to the best knowledge of the authors, our paper is the first to use an SIW antenna for the proposed sectorized radar to achieve a complete horizontal FOV of $-90°$ to $+90°$ and with a high operating bandwidth of more than 6% (see Table 1).

A. TRANSMIT SUBSTRATE INTEGRATED WAVEGUIDE (SIW) ANTENNAS

SIW antennas generally have decreasing impedance bandwidth with a higher number of radiating slots [54]. However, the investigated structure employs three slots which not only increases the gain and bandwidth of the antenna but generates a fan-like far field beampattern in the horizontal plane. This is important such that a large angular range is illuminated by the transmitter. For example, the achieved half-power beamwidth is about 60 degrees. Also, the measured -10 dB impedance bandwidth of the TX-SIW (see Fig. 11, left) was more than 1.5 GHz centered at 23.75 GHz (all results not reported for brevity).

The three radiating slots determine the transmit antenna fan-like beam in the horizontal plane and the fabricated TX-SIW can be seen in Fig. 11 (left) and its beampattern is observed in Fig. 12. It should be mentioned that results for two transmitter prototypes are reported, and as can be observed, similar results are shown with general agreement with the full-wave simulations. This beampattern characteristic allows the radar to have a wide coverage of the FOV in the transmit path, assuring electromagnetic scattering returns back from the targets at the required angles.
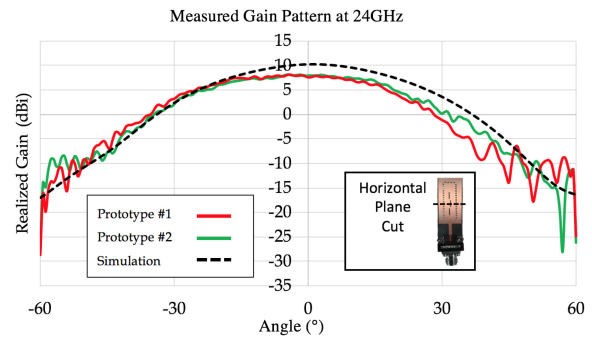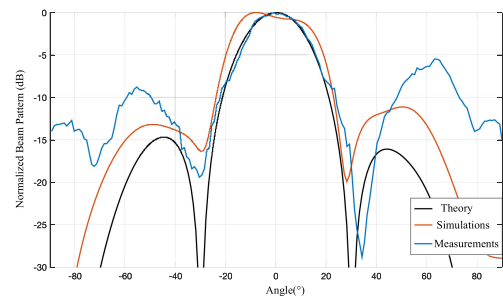
B. RECEIVE SUBSTRATE INTEGRATED WAVEGUIDE (SIW) ANTENNA ARRAYS AND DUAL-MODE DETECTION

In the receiver configuration, the designed SIW structure uses an array of longitudinal slots. As with the transmit antennas, the design parameters have been selected according to the guidelines presented in [55], [56] and optimised using CST Microwave Studio. The beam pattern measurements of both the transmit and the receive antennas were completed in a calibrated anechoic chamber using a near-field system (NSI) positioner which computed the far-field response of the antennas. Good agreement between CST simulations and the measurements can be observed for the S-parameters and impedance matching values of less than -10 dB are observed for the 8-port structure with a bandwidth of about 2 GHz (in Fig. 11, right, all results not reported for brevity). Also, the horizontal patterns of the four-element array at $\lambda/2$ inter-element spacing is shown in Fig. 13.

The half-power beamwidth of the λ-spaced receiver is reduced by approximately a factor of two when compared to the $\lambda/2$ spaced receiver due to the enlarged aperture, but it introduces grating lobes. The investigation of these two configurations can allow for the same target scenario to be viewed by the radar system to obtain useful data from both resolution perspectives. Consequently, this makes it advantageous to interrogate data from both radar receiver configurations because each set has acquired complementary data for each radar measurement. Therefore, combining data with such a two-fold detection system (see Fig. 14)) can offer improved
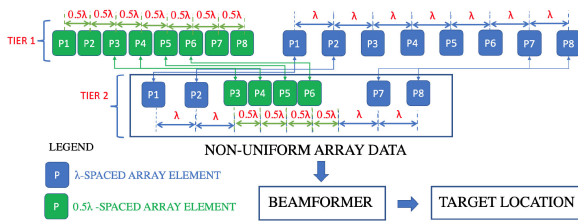
FIGURE 14. Two-tier process for determining the sparse, non-uniform antenna from MIMO data for $\lambda/2$ and λ-spacing.

angular resolution for the radar should that be desired. Since our presented radar uses an antenna array which can detect at both $\lambda/2$ and λ spacing (respectively RP3, RP4, RP5, and RP6, and, RP1 $\cdots$ RP8, defining Tier 1, see Fig. 14), we have used this two-tier approach to investigate further the possibility of improved angular resolution.

The employed method for obtaining the non-uniform antenna array (Tier 2) is to search through the antenna beampattern responses which result in an improved $\Theta_{3\,dB}$ and SLL by combining both $\lambda/2$ data and λ data. By removing unnecessary elements that contribute to the grating lobes and increased SLL, we are able to obtain an improved array pattern. However, this exhaustive search implies evaluating the patterns of over 10,000 antenna array configurations. To overcome this challenging selection, an automated methodology in MAT-LAB was developed to identify the best antenna array combination of $\lambda/2$ data and λ data, where the algorithm would choose only solutions which have improved $\Theta_{3\,dB}$ and SLL compared to the previous solution. An overview of this two-tier process is illustrated in Fig. 14, which also shows the best antenna configuration for our proposed sparse antenna array design.

Fig. 15 depicts the 8-element receiver antenna connections. A similar procedure was adopted for the modular MIMO radar (see Fig. 4(c)) realising the effective 32-element receiver. This MIMO radar antenna configuration has a virtual aperture length of 23.5λ, which is equivalent to a virtual array of 47 antenna elements with a spacing of $\lambda/2$ defining the effective receiver. Therefore, a reduction in the number of elements by 32% is achieved by employing just 32 elements when compared to an equivalent aperture size of 47. Further discussions on the analysis and measurements for these SIW antennas will be described next considering the different spaced arrays. The interested reader can see [57]–[59] for more information on sparse arrays and MIMO radar concepts.

The employed SIW antenna arrays exhibits less radiation on the edges of the PCB contributing to the element beampattern when compared to a more omnidirectional-like antenna. Therefore, the total antenna receiver array response for the RMs will also exhibit lower radiation levels on the edges of the antennas and in the positions of the grating lobes (when considering the far-field). We show the numerically calculated array factors in Figs. 16 and 17 for 8-elements and 32-elements. Notice the relatively high grating lobes at $\pm 90°$ for the λ-spaced array as well as the non-uniform sparse array.

These results can be compared to the measurements found in Figs. 18 and 19 using the measured element factor and the calculated array response. As it can be observed, the grating lobes and the first side-lobe for the λ-spaced receiver do not appear as high when compared to the calculated array factors in Figs. 16 and 17. Similarly, for the non-uniform sparse array. For example, pattern levels are about -15 dB below the main beam maximum in both cases. This is due to the minimal radiation at the PCB edges for the SIW antenna elements as described earlier as well as the optimized element positioning for the sparse array having non-uniform spacing.

VI. RADAR SYSTEM MEASUREMENTS
The radar architecture for proof-of-concept has been tested in an anechoic chamber. Several trials have been carried out to verify: range approximation, range resolution and angle of arrival estimation with delay-and-sum digital beamforming. In general, theoretical findings, simulation studies, and radar system measurements are in agreement. The experiments included a SIMO setup for radar range testing as well as three RMs (see in Figs. 20(a) and (b)), which were assigned to each sector of the FOV. This meant multiple readings were required to achieve the effective virtual apertures for the modular MIMO radar and the sectorized radar systems as outlined previously (see Fig. 4). Also, as shown in Fig. 20(c), three square metallic targets have been used with different sizes during the experiments. A photograph of the angular detection trial can be seen in Fig. 20(d).

A. TARGET DETECTION MEASUREMENT SETUP
Radar detection of the targets was first measured using a SISO configuration (see Fig. 4(a)). As can be seen from Fig. 21, both the targets (30 cm $\times$ 30 cm and 20 cm $\times$ 20 cm) are visible for a 13 cm separation. Another test has been carried out for the target separation below 10 cm and the two targets were not distinguishable. This experiment confirms that the range resolution of the radar is approximately 10 cm. This is because for a 1.5 GHz radar bandwidth (BW), we can observe a theoretical range resolution of $v_0 / (2\,\text{BW})$ where $v_0 = 3.0 \times 10^8$ m/s. This is also confirmed by our simulations (see Fig. 21). Furthermore, a target has been swept at several distances up to 4 meters in order to check the range accuracy at both 250 MHz and 1.5 GHz. Results are reported in Fig. 22 where it can be observed that the radar was able to track the target in range. Also, with increased radar BW, it can be observed that the measured range accuracy improved. These results follow the expected response of the radar system.

B. TARGET ANGULAR ESTIMATES
Measurements have been carried out for $\lambda/2$-spaced, λ-spaced and non-uniform sparse receiver configurations. Since each RM is defined by using only two transmitters and four receivers, the measurements for the 32-element virtual receiver array, for each sector, have been carried out by displacing the MIMO RMs at positions of exactly 4λ from each other (similar to how a synthetic aperture radar would acquire its
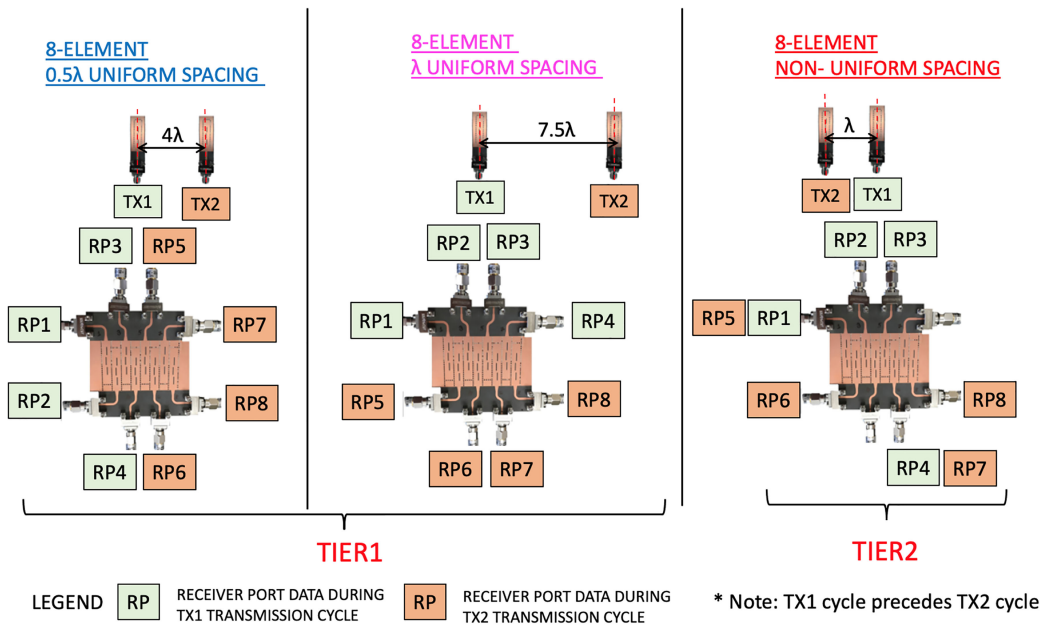
FIGURE 15. Radar receiver configurations for 8-element ¹/₂, λ-spaced and the non-uniform MIMO array receiver using SIW receiver antennas.
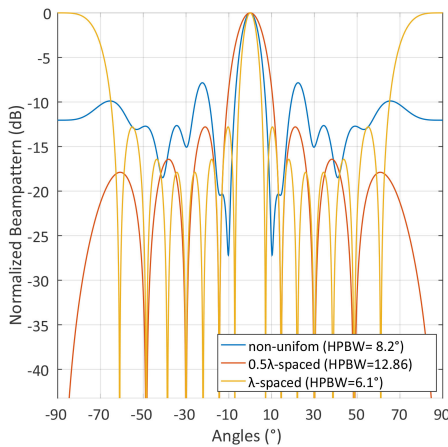

FIGURE 16. Numerically calculated array factor for the RM considering 8 elements at ¹/₂ uniform spacing, λ uniform spacing, and sparse non-uniform spacing.
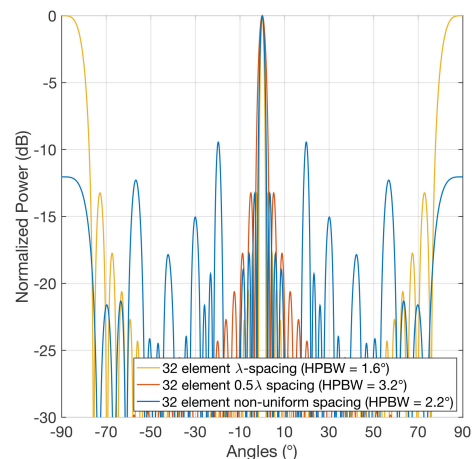

FIGURE 17. Numerically calculated array factor for 32 elements at ¹/₂ uniform spacing, λ uniform spacing, and sparse non-uniform spacing.

data). This measurement approach and by considering the same target scenario, has permitted the authors to predict the performance of the modular MIMO radar system for the 32-element virtual receiver array, whilst considering both uniform and non-uniform spacing.

The results of the measurements with one target as well as two targets spaced at different angular separations are shown in Figs. 23, 24, 25 and 26. For the multiple target scenarios, the targets have been measured while spaced at decreasing offsets of 2° in order to observe the responses. The results show that the radar with non-uniform spacing is managing to detect both targets in all situations, even when these targets are spaced at an angular distance of ±2°. Also, the side-lobe levels (SLLs) are about 8 dB below (or better) from the main

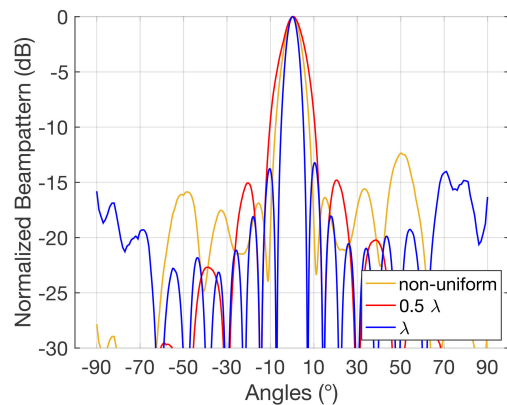**FIGURE 18.** Measurement comparison of the 8 element MIMO radar antenna considering ¹/₂ uniform spacing, λ uniform spacing, and the non-uniform sparse array.
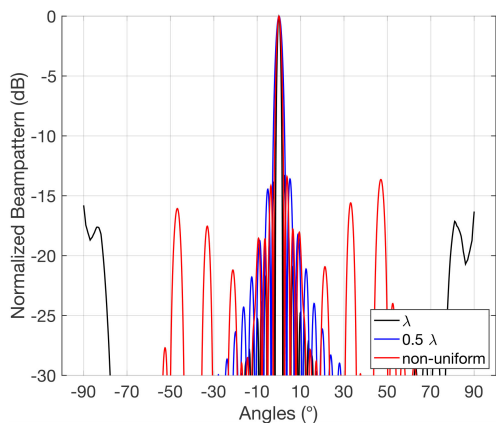
FIGURE 19. Measurement comparison of the measured 32 element MIMO radar antenna for $\lambda/2$ uniform spacing, λ uniform spacing, and the non-uniform sparse array configuration.

(a) SIMO RADAR Antenna Alignment

(b) Three Sector Radar Hardware Set-up

(c) Square Metallic Targets: 10 cm x 10 cm, 20 cm x 20 cm, 30 cm x 30 cm

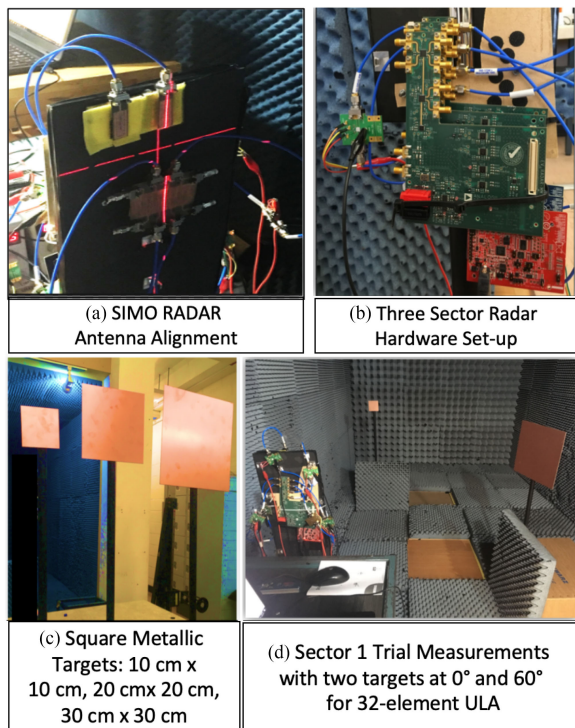(d) Sector 1 Trial Measurements with two targets at 0° and 60° for 32-element ULA

FIGURE 20. Measurement setup for the radar detection trials within an anechoic chamber with 3 RMs and three targets of dimensions: 10 cm $\times$ 10 cm, 20 cm $\times$ 20 cm and 30 cm $\times$ 30 cm.

FIGURE 21. Range resolution simulations and measurements with two targets separated above and below the angular resolution limit of 10 cm using a 1.5 GHz antenna transmitter bandwidth.

FIGURE 22. Range accuracy comparison using one target for a distance up to 4 meters using a 250 MHz and 1.5 GHz bandwidth.
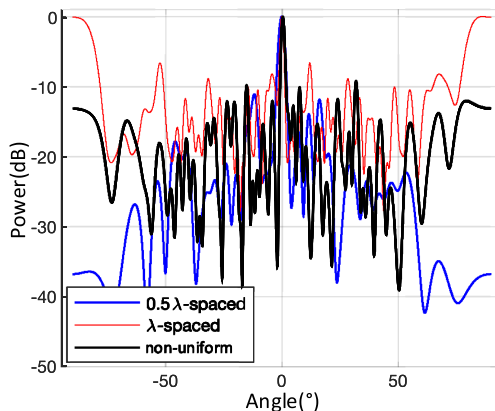
FIGURE 23. One target comparison: $\lambda/2$, λ and non-uniform spacing.

target estimates for the angular spectrums. In addition, it can be observed that the grating lobes are mitigated at about $\pm 90°$ for the non-uniform spaced array when compared to the λ-spaced receiver. For example, grating lobes are reduced to about -12 dB (or more) in Fig. 23 for the non-uniform array. Similar results are observed in Figs. 24, 25, and 26.

There are a few possible strategies to improve the SLLs for the radar system should it be desired. One solution as mentioned in [60], is to apply time-domain spectral smoothing [61] to allow several images of the radar to be averaged. This technique is si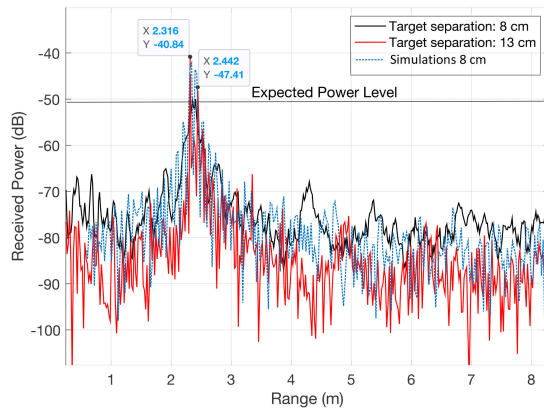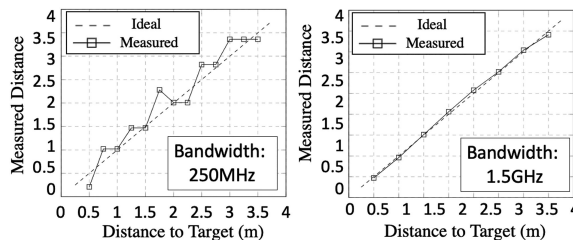milar to the averaging of multiple frequency-domain samples when completing vector network analyzer (VNA) measurements for low power signals in a noisy environment, or, when reducing the IF bandwidth on a spectrum analyser making the noise floor decrease (or improving the signal-to-noise ratio; i.e. the SNR), however, at the cost of increased measurement time. This can result in a cleaner or more accurate response where this noise level is reduced, in practice, improving the SNR when considering a practical radar setup.

Following [61] this spectral smoothing approach has been shown to practically improve the radar detection accuracy. For example, in [60], 2 targets (with a narrow $\pm 1°$ angular

FIGURE 24. Radar measurement comparison for an 8 ° angular target separation: λ/2, λ and non-uniform spacing. It should be mentioned that gra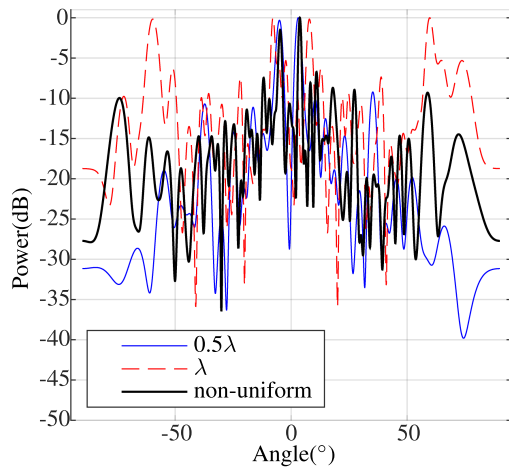ting lobes are observed for the λ spaced array at about ±60° while the radar measurement with the non-uniform receiver array clearly distinguishes the targets and where grating lobes and SLLs are about −10 dB or lower.
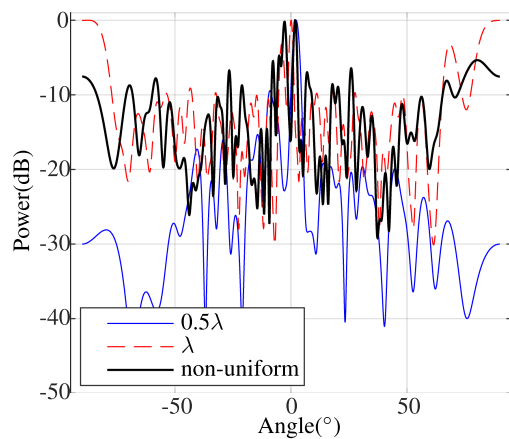

FIGURE 25. Radar measurement comparison for a 6 ° angular target separation: λ/2, λ and non-uniform spacing, which, is the only effective radar antenna which can clearly distinguish the two targets; i.e. the non-uniform spaced array.

FIGURE 26. Radar measurement comparison for a 4 ° (or ±2 degrees) angular target separation: λ/2, λ and non-uniform spacing. Again, similar to Fig. 25, the non-uniform spaced array is the only virtual receiver than can decipher the two targets and with low SLLs for the angular spectrum estimate.

SLL mitigation is probable for the complete radar system. Basically, by using the noted spectral smoothing made possible by additional measurement sampling and post-processing of the radar responses, our findings suggest that the accuracy of the angular target estimates can be improved (see for example, results in [62] for an individual RM, results not reported herein for multiple RMs due to brevity). Regardless, we would like to highlight that a more dedicated study is required to investigate this spectral smoothing methodology within our modular radar system compromised of many RMs and this defines future work.

This is because our findings in this paper suggest that additional noise is apparent in the measured radar system, due to the tiling of the multiple RMs and when compared to just the individual radar arrays. Basically, the SNR decreases for the complete radar response and this could be due to unwanted mechanical misalignment of the RMs when completing the laboratory measurements for the proof-of-concept radar system, or, the noise generated by the microwave circuits (i.e. the radar circuit hardware: VCO, mixers, amplifiers, etc.) within the RMs themselves. Moreover that, when the RMs work collectively and are networked, practical noise levels increase for the radar and this was studied statistically in MATLAB and these simulations confirm these findings (results not reported due to brevity). Basically, these noted practicalities can decrease the SNRs from less than −20 dB (for the simulations) to between −12 and −15 dB for the physical target angular estimates in a controlled microwave laboratory setting. Therefore, these noted practicalities can diminish the collective radar system (which is comprised of multiple RMs) when compared to an ideal radar setup, as well as, a practical radar defined by an individual RM.

This can be further identified by observing the SLL for the 8-port antenna measurements in Fig. 18 which are below −15 dB for the non-uniform sparse array. The grating lobes are also mitigated in these measurements and this can be

separation) where resolved when spectral smoothing was applied using an advanced SIW buttler matrix beamformer at the FMCW transmitter, and with, time-domain beam steering. Similarly, this spectral smoothing has also shown an improvement of 13 dB for the SLL of the radar system as reported in [62]. Other possible solutions for SLL reduction when considering the employed SIW arrays, and likely SNR improvement for the complete radar, include the use of tapering functions such as Gaussian, Chebyshev, Hamming, or Taylor window functions for the radar antenna aperture [22], [63]. However, these approaches can tend to broaden the half-power beamwidth of the array and thus possibly diminish the angular resolution of the radar which might be unwanted.

Given these above discussions, the mathematical foundations outlined in [61], and our previous findings [60], [62],
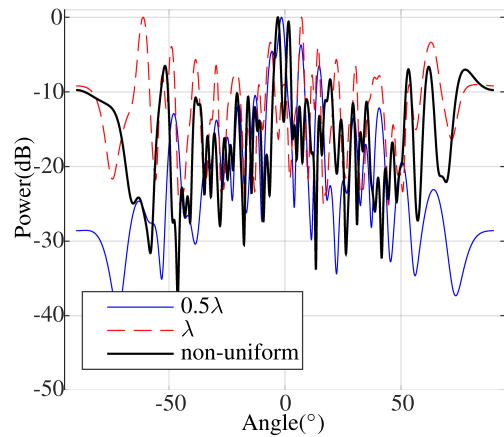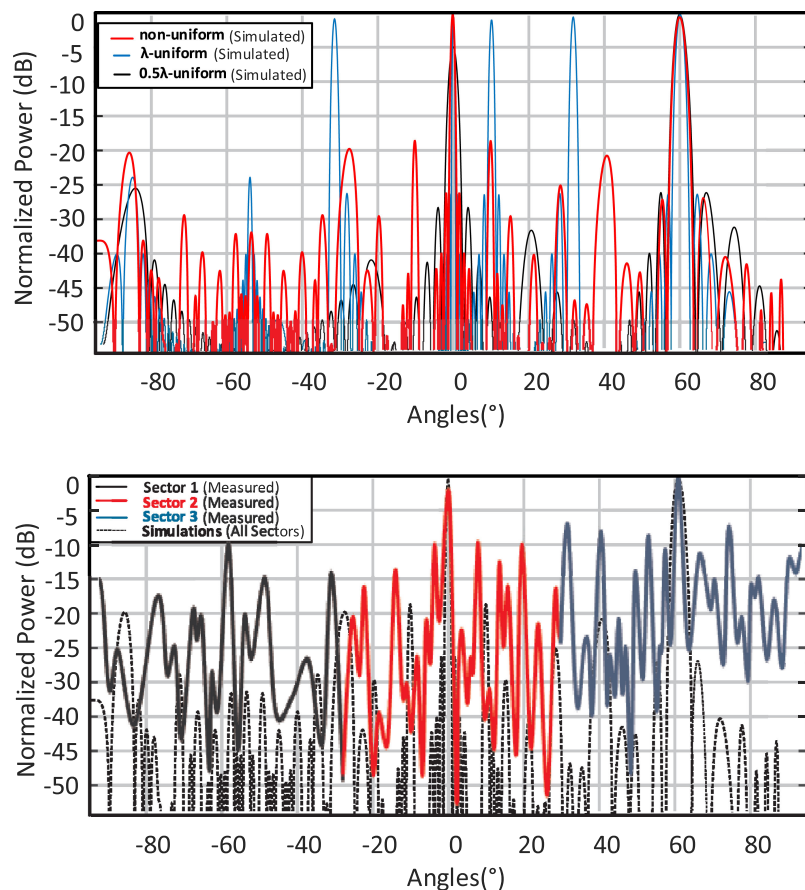
FIGURE 27. Simulation results (a), as well as, simulations compared to measurements (b), for a sectorized radar trial detecting two targets at 0° and 65° as identified in Fig. 20(d). The targets have been placed at an angular separation of 65° to highlight the improvement of the sparse array approach, see (b) for the simulations and measurements for each sector, as compared to the simulated $\lambda/2$-spaced and λ-spaced uniform array in (a).

observed when inspecting the array factors themselves (see Fig. 16) for the λ-spaced array as well as the non-uniform sparse array. However, when four RMs are arranged to work collectively, the radar SNR decreases to a range from about −8 dB to −13 dB (see Figs. 23, 24, 25 and 26). In general, these SLL and SNR metrics are important for automotive radar scenarios because high levels (i.e. about −10 dB) could bring some ambiguity and reduced accuracy for the radar, or suggest false targets near a main one. It should also be mentioned that there are few works which manage to achieve a radar SLL value of more than about −12 dB (see Table 1). This implies that there needs to be a consistent effort across academia and industry to improve this metric, whilst preserving high angular resolution and system BW as well as minimizing implementation costs, radar architecture complexity, and signal processing time for the complete radar system. As mentioned previously, these were the design motivations for this work.

C. SECTORIZED MIMO RADAR SYSTEM RESULTS

Most radar systems assume that a single radar covers the FOV in the horizontal plane. The proposed sectorized MIMO radar system, on the other hand, presents a novel and improved solution to previous radar works (see Table 1) by employing multiple RMs in order to discretely sample the angular space. The front horizontal plane of the radar can be divided into three sectors allowing for precise detection (see Fig. 4(d)). Moreover, this allows for data to be sampled at each RM, giving a combined response for the three sectors by data fusion. Results are shown in Fig. 27 and further details for the experiment are described herein.

Each of the modular MIMO radars for each sector is defined by a 32-element virtual receiver array with non-uniform spacing as described in the previous sections. Since the switching speed of the RF ports is completed in approximately 50 ns between each transmitter, the total switching time for the radar system is estimated to be 1.2 μs. Also, the time required to process the targets by the beamforming algorithm varies between 22 ms and 30 ms for each sector.

The computer hardware used for this data processing is performed using a laptop running MATLAB. In particular, the computer characteristics are as follows: a 2.6 GHz Dual-Core Intel Core i5 processor (I5-4278 U), with 8 GB of DDR3 memory, using an Intel Iris graphics card of 1.5 GB. It is expected that the performance can be improved if the system is transitioned to FPGA-based processing. The modular MIMO radars, see Figs. 4(c and d), are also tilted which are representative of the final front-end configuration, so that

non-overlapping horizontal coverage can be obtained uniformly for the combined radar views. If the radar beams would overlap then it is possible to see some unexpected effects in detection due to the possible interference cause by the adjacent radars.

Figs. 27(a) and (b) show how multiple RMs extend the horizontal coverage of the radar system and that non-uniform spacing can avoid false target detection. This figure highlights two targets consisting of one larger metal plate (30 cm × 30 cm) at 60° from the middle line of the radar system at a 2.5 m distance, while the smaller (20 cm × 20 cm) is situated at 4 m distance at the middle line of the radar. Also, the non-uniform spaced antenna configuration eliminates the grating lobe issue. It can be seen from the simulation results of the scenario, depicted in Fig. 27(a), how the λ-spaced antenna arrays suffer from grating lobes. The particularity of this detection, which has been measured in Fig. 27(b), is that the targets which appear farther in one section are closer for the other section, hence the target at 65° has also the received power of a target detected at its broadside for the modular MIMO radar observing sector 3. All in all, it can be seen that the non-uniform sparse approach presents higher performance than the other solutions presented.

D. GENERAL DISCUSSIONS FOR THE SECTORIZED RADAR

In comparison to the mentioned literature [3]–[7], [14], the radar presented in this paper proposes maximum performance in all areas of detection in terms of ±90° FOV, angular resolution Θ_{3dB}, and detection time (see Table 1). Increased receiver sensor separation improves the angular resolution of the radar while range resolution is improved by the operating bandwidth of the employed SIW antennas. When used appropriately, the modular MIMO radars can maximize FOV for the three sectors while targets are rapidly detected due to the simple digital beamforming method and MIMO processing. To the best knowledge of the authors, this paper is the first to produce a sectorized MIMO radar architecture which achieves full coverage of the horizontal plane (±90°) using numerous sub-arrays and MIMO RMs which supports low-cost mass production rather than the assembly and manufacturing of a larger scale and equivalent radar system with the same number of receiver elements.

VII. CONCLUSION

The paper presents a MIMO radar system architecture which achieves high range resolution while being the first to report far-field measurements of ±90° coverage for a short-range radar system. Also, the measured radar system offers more than a 6% bandwidth (see Table 1) with FMCW signal transmission at 24 GHz for proof-of-concept demonstration. It should also be mentioned that our proposed radar design is scalable, in that it could be re-designed to operate at 77 GHz for example, or any microwave or millimetre-wave frequency for that matter, assuming the relevant radar antennas and electronics are available, and, with the appropriate bandwidth whilst complying with any transmission requirements and allowable frequency allocations. Possible applications include

autonomous vehicle and automotive radar. Despite increased signal processing requirements due to the multiple radar sub-modules and data fusion for the three sectors, competitive processing times (see Table 1) of about 30 ms or less are observed. Also, the angular resolution achieved by the non-uniform sectorized two-mode MIMO radar is better than the standard $\lambda/2$-spaced array, offering an experimentally verified half-power beamwidth of 2.2°.

It should also be mentioned, that by employing the aforementioned radars, channel noise and signal delays are reduced to a minimum in comparison with a larger scale and more conventional transmit and receiver array, mainly due to the fact that a microstrip-based corporate feeding network or other large-scale beam forming networks (i.e. a Rotman lens for example) are not required. In summary, the presented system design allows for individual sub-sector sampling enabling a modular and sectorized MIMO radar approach. This can support the development of new beamforming techniques for automotive short-range radars which offer reduced SLL, grating lobe mitigation, reduced noise, and competitive range and angle target resolution.

REFERENCES

[1] Centre for Connected & Autonomous Vehicles, "U.K. connected & autonomous vehicle research & development projects 2018," 2018. [Online]. Available: https://bit.ly/2ERwDgb

[2] Centre for Connected & Autonomous Vehicles, "Market forecast for connected & autonomous vehicles," 2017. [Online]. Available: https://bit.ly/2CCvZkj

[3] B.-H. Ku et al., "A 77-81 GHz 16-element phased-array receiver with ±50° beam scanning for advanced automotive radars," *IEEE Trans. Microw. Theory Techn.*, vol. 62, no. 11, pp. 2823–2832, Nov. 2014.

[4] J. Hasch, E. Topak, R. Schnabel, T. Zwick, R. Weigel, and C. Waldschmidt, "Millimeter-wave technology for automotive radar sensors in the 77 GHz frequency band," *IEEE Trans. Microw. Theory Techn.*, vol. 60, no. 3, pp. 845–860, Mar. 2012.

[5] M. Steinhauer, H.-O. Ruob, H. Irion, and W. Menzel, "Millimeter-wave-radar sensor based on a transceiver array for automotive applications," *IEEE Trans. Microw. Theory Techn.*, vol. 56, no. 2, pp. 261–269, Feb. 2008.

[6] R. Feger, C. Wagner, S. Schuster, S. Scheiblhofer, H. Jager, and A. Stelzer, "A 77-GHz FMCW MIMO radar based on an SiGesingle-chip transceiver," *IEEE Trans. Microw. Theory Techn.*, vol. 57, no. 5, pp. 1020–1035, May 2009.

[7] R. Feger, C. Pfeffer, and A. Stelzer, "A frequency-division MIMO FMCW radar system based on delta-sigma modulated transmitters," *IEEE Trans. Microw. Theory Techn.*, vol. 62, no. 12, pp. 3572–3581, Dec. 2014.

[8] C. Alistarh et al., "Millimetre-wave FMCW MIMO radar system development using broadband SIW antennas," in *Proc. 12th Eur. Conf. Antennas Propag.*, 2018, pp. 1–5.

[9] D. Mateos-Núñez, M. A. González-Huici, R. Simoni, F. B. Khalid, M. Eschbaumer, and A. Roger, "Sparse array design for automotive MIMO radar," in *Proc. 16th Eur. Radar Conf.*, 2019, pp. 249–252.

[10] C. M. Schmid, R. Feger, C. Wagner, and A. Stelzer, "Design of a linear non-uniform antenna array for a 77-GHz MIMO FMCW radar," in *Proc. IEEE MTT-S Int. Microw. Workshop Wireless Sensing, Local Positioning, RFID*, 2009, pp. 1–4.

[11] R. Rajamäki and V. Koivunen, "Comparison of sparse sensor array configurations with constrained aperture for passive sensing," in *Proc. IEEE Radar Conf.*, 2017, pp. 0797–0802.

[12] S. Kueppers, H. Cetinkaya, and N. Pohl, "A compact 120 ghz SiGe: C based 2× 8 FMCW MIMO radar sensor for robot navigation in low visibility environments," in *Proc. IEEE Eur. Radar Conf.*, 2017, pp. 122–125.

[13] H. J. Ng, W. Ahmad, and D. Kissinger, "Scalable MIMO radar utilizing delta-sigma modulation-based frequency-division multiplexing technique," in *Proc. IEEE Eur. Radar Conf.*, 2017, pp. 118–121.

[14] J. Massen, M. Frei, W. Menzel, and U. Möller, "A 79 GHz SiGe short-range radar sensor for automotive applications," *Int. J. Microw. Wirel. Technol.*, vol. 5, no. 1, pp. 5–14, Jan. 2013.

[15] L. Daniel *et al.*, "Application of Doppler beam sharpening for azimuth refinement in prospective low-THz automotive radars," *IET Radar, Sonar Navig.*, vol. 12, no. 10, pp. 1121–1130, Sep. 2018.

[16] S. Gishkori, L. Daniel, M. Gashinova, and B. Mulgrew, "Imaging for a forward scanning automotive synthetic aperture radar," *IEEE Trans. Aerosp. Electron. Syst.*, vol. 55, no. 3, pp. 1420–1434, Jun. 2019.

[17] D. Jasteh, E. Hoare, M. Cherniakov, and M. Gashinova, "Experimental low-terahertz radar image analysis for automotive terrain sensing," *IEEE Geosci. Remote Sens. Lett.*, vol. 13, no. 4, pp. 490–494, Apr. 2016.

[18] ETSI Technical Committee, "Electromagnetic compatibility and radio spectrum matters (ERM); SRD radar equipment using wideband low activity mode (WLAM) and operating in the frequency range from 24,05 GHz to 24,50 GHz TR 102 892 v1.1.2 (2011-07)," Tech. Rep., 2011.

[19] Y.-S. Won, C.-H. Kim, and S.-G. Lee, "Range resolution improvement of a 24 GHZ ISM band pulse radar-a feasibility study," *IEEE Sensors J.*, vol. 15, no. 12, pp. 7142–7149, Dec. 2015.

[20] W. Mayer, A. Gronau, W. Menzel, and H. Leier, "A compact 24 GHZ sensor for beam-forming and imaging," in *Proc. IEEE 9th Int. Conf. Control, Autom., Robot. Vis.*, 2006, pp. 1–6.

[21] C.-Y. Ho, S.-C. Hsieh, M.-F. Jhong, H.-C. Kuo, C.-Y. Ting, and C.-C. Wang, "A low-cost antenna-in-package solution for 77 GHZ automotive radar applications," in *Proc. Int. Conf. Electron. Packag.*, 2019, pp. 110–114.

[22] M. I. Skolnik, *Radar Handbook*, 2nd ed., Illinois, CA, USA: McGraw Hill, 2000.

[23] M. I. Skolnik, *Introduction to Radar Systems*. New York, NY, USA: McGraw-Hill, 2007.

[24] M. Cheney and B. Borden, *Fundamentals of Radar Imaging*, ch. 4. Society for Industrial and Applied Mathematics, 2009. [Online]. Available: https://epubs.siam.org/doi/abs/10.1137/1.9780898719291

[25] V. Perrot, M. Polichetti, F. Varray, and D. Garcia, "So you think you can DAS? A viewpoint on delay-and-sum beamforming," *Ultrasonics*, vol. 111, 2021, Art. no. 106309.

[26] S. M. Patole, M. Torlak, D. Wang, and M. Ali, "Automotive radars: A review of signal processing techniques," *IEEE Signal Process. Mag.*, vol. 34, no. 2, pp. 22–35, Mar. 2017.

[27] G. Hakobyan and B. Yang, "High-performance automotive radar: A review of signal processing algorithms and modulation schemes," *IEEE Signal Process. Mag.*, vol. 36, no. 5, pp. 32–44, Sep. 2019.

[28] S. Sun, A. P. Petropulu, and H. V. Poor, "MIMO radar for advanced driver-assistance systems and autonomous driving: Advantages and challenges," *IEEE Signal Process. Mag.*, vol. 37, no. 4, pp. 98–117, Jul. 2020.

[29] C. Waldschmidt, J. Hasch, and W. Menzel, "Automotive radar-from first efforts to future systems," *IEEE J. Microwaves*, vol. 1, no. 1, pp. 135–148, Jan. 2021.

[30] J. Grythe, "Beamforming algorithms-beamformers," *Tech. Note, Norsonic AS*, 2015.

[31] S. Rao, *MIMO Radar*. Texas Instruments, USA, 2017.

[32] C. Vasanelli *et al.*, "Calibration and direction-of-arrival estimation of mm-wave radars: A practical introduction," *IEEE Antennas Propag. Mag.*, vol. 62, no. 6, pp. 34–45, Dec. 2020.

[33] J. Li and P. Stoica, "Mimo radar with colocated antennas," *IEEE Signal Process. Mag.*, vol. 24, no. 5, pp. 106–114, Sep. 2007.

[34] I. Bilik *et al.*, "Automotive MIMO radar for urban environments," in *Proc. IEEE Radar Conf.*, 2016, pp. 1–6.

[35] F. Engels, M. Wintermantel, and P. Heidenreich, "Automotive MIMO radar angle estimation in the presence of multipath," in *Proc. IEEE Eur. Radar Conf.*, 2017, pp. 82–85.

[36] C. Pfeffer, R. Feger, C. Wagner, and A. Stelzer, "FMCW MIMO radar system for frequency-division multiple TX-beamforming," *IEEE Trans. Microw. Theory Techn.*, vol. 61, no. 12, pp. 4262–4274, Dec. 2013.

[37] E. Fishler, A. Haimovich, R. Blum, D. Chizhik, L. Cimini, and R. Valenzuela, "MIMO radar: An idea whose time has come," in *Proc. IEEE Radar Conf.*, 2004, pp. 71–78.

[38] J. Li and P. Stoica, *MIMO Radar Signal Processing*. Hoboken, NJ, USA: Wiley, 2008.

[39] B. Schweizer, C. Knill, D. Schindler, and C. Waldschmidt, "Stepped-carrier OFDM-radar processing scheme to retrieve high-resolution range-velocity profile at low sampling rate," *IEEE Trans. Microw. Theory Techn.*, vol. 66, no. 3, pp. 1610–1618, Mar. 2018.

[40] C. Knill, B. Schweizer, S. Sparrer, F. Roos, R. F. Fischer, and C. Waldschmidt, "High range and Doppler resolution by application of compressed sensing using low baseband bandwidth OFDM radar," *IEEE Trans. Microw. Theory Techn.*, vol. 66, no. 7, pp. 3535–3546, Jul. 2018.

[41] D. Schindler, B. Schweizer, C. Knill, J. Hasch, and C. Waldschmidt, "MIMO-OFDM radar using a linear frequency modulated carrier to reduce sampling requirements," *IEEE Trans. Microw. Theory Techn.*, vol. 66, no. 7, pp. 3511–3520, Jul. 2018.

[42] W. Deng, R. Mahmoudi, and A. H. Van Roermund, *Time Multiplexed Beam-Forming With Space-Frequency Transformation*. Berlin, Germany: Springer, 2012.

[43] A. M. Haimovich, R. S. Blum, and L. J. Cimini, "MIMO radar with widely separated antennas," *IEEE Signal Process. Mag.*, vol. 25, no. 1, pp. 116–129, Jan. 2008.

[44] G. Rubio-Cidre, A. Badolato, L. Úbeda-Medina, J. Grajal, B. Mencia-Oliva, and B.-P. Dorta-Naranjo, "DDS-based signal-generation architecture comparison for an imaging radar at 300 GHz," *IEEE Trans. Instrum. Meas.*, vol. 64, no. 11, pp. 3085–3098, Nov. 2015.

[45] B.-G. Goldberg, *Digital Frequency Synthesis Demystified*. New York, NY, USA: Elsevier, 2000.

[46] ADF4159 Data Sheet, "Direct modulation/fast waveform generating, 13 GHz, fractional-N frequency synthesizer."

[47] Y. Chong and D. Wenbin, "Microstrip series fed antenna array for millimeter wave automotive radar applications," in *Proc. IEEE MTT-SIMWS Int. Microw. Workshop Ser. mm-Wave Wireless Technol. Appl.*, 2012, pp. 1–3.

[48] Y. Dong and T. Itoh, "Planar ultra-wideband antennas in Ku-and K-band for pattern or polarization diversity applications," *IEEE Trans. Antennas Propag.*, vol. 60, no. 6, pp. 2886–2895, Jun. 2012.

[49] L. S. Locke, J. Bornemann, and S. Claude, "Substrate integrated waveguide-fed tapered slot antenna with smooth performance characteristics over an ultra-wide bandwidth," *Appl. Comput. Electromagn. Soc. J.*, vol. 28, pp. 454–462, Aug. 2012.

[50] K. Wu, M. Bozzi, and N. J. Fonseca, "Substrate integrated transmission lines: Review and applications," *IEEE J. Microwaves*, vol. 1, no. 1, pp. 345–363, Jan. 2021.

[51] W. Menzel, "Antennas in automobile radar," in *Handbook of Antenna Technologies*. Berlin, Germany: Springer, 2014, pp. 1–22.

[52] N. J. G. Fonseca, A. Ali, and H. Aubert, "Cancellation of beam squint with frequency in serial beamforming network-fed linear array antennas," *IEEE Antennas Propag. Mag.*, vol. 54, no. 1, pp. 32–39, Feb. 2012.

[53] R. Garg, I. Bahl, and M. Bozzi, *Microstrip Lines and Slotlines*. Norwood, MA, USA: Artech House, 2013.

[54] M. Bozzi, A. Georgiadis, and K. Wu, "Review of substrate-integrated waveguide circuits and antennas," *IET Microw. Antennas Propag.*, vol. 5, no. 8, pp. 909–920, Dec. 2010.

[55] F. Xu and K. Wu, "Guided-wave and leakage characteristics of substrate integrated waveguide," *IEEE Trans. Microw. Theory Techn.*, vol. 53, no. 1, pp. 66–73, Jan. 2005.

[56] T. A. Milligan, *Modern Antenna Design*. Hoboken, NJ, USA: Wiley, 2005.

[57] A. Dürr *et al.*, "On the calibration of mm-wave MIMO radars using sparse antenna arrays for DoA estimation," in *Proc. 16th Eur. Radar Conf.*, 2019, pp. 349–352.

[58] S. Sedighi, B. Shankar, K. V. Mishra, and B. Ottersten, "Optimum design for sparse FDA-MIMO automotive radar," in *Proc. 53rd Asilomar Conf. Signals, Syst., Comput.*, 2019, pp. 913–918.

[59] D. Mateos-Núñez *et al.*, "Sparse array design for automotive MIMO radar," in *Proc. 16th Eur. Radar Conf.*, 2019, pp. 249–252.

[60] P. D. H. Re *et al.*, "FMCW radar with enhanced resolution and processing time by beam switching," *IEEE Open J. Antennas Propag.*, vol. 2, pp. 882–896, 2021.

[61] J. K. Kauppinen, D. J. Moffatt, H. H. Mantsch, and D. G. Cameron, "Smoothing of spectral data in the Fourier domain," *Appl. Opt.*, vol. 21, no. 10, pp. 1866–1872, 1982.

[62] C. A. Alistarh, S. K. Podilchak, G. Goussetis, J. S. Thompson, and J. Lee, "Spectral smoothing by multiple radar pattern multiplication for improved accuracy," in *Proc. IEEE 18th Int. Symp. Antenna Technol. Appl. Electromagn.*, 2018, pp. 1–2.

[63] C. A. Balanis, *Antenna Theory: Analysis and Design*. Hoboken, NJ, USA: Wiley, 2016.
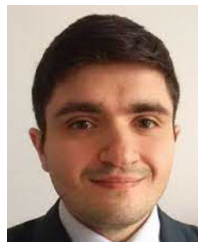
CRISTIAN A. ALISTARH (Graduate Student Member, IEEE) received the M.Eng. degree in electronics and computer science from The University of Edinburgh, Edinburgh, U.K., in 2015, as a Keycom Scholar, and the joint M.Sc. degree in sensors and imaging systems from the University of Glasgow, Glasgow, U.K., and the University of Edinburgh, sponsored by the Scottish Council in the U.K. Since 2017, he has been working toward the joint Ph.D. degree with Heriot-Watt University, Edinburgh, U.K., together with the University of Edinburgh in partnership with Samsung Research and Development, South Korea. His research interests include high resolution automotive radar, MIMO systems, digital beamforming, sparse antenna design, and compressed sensing.

Mr. Alistarh was shortlisted for Best Paper in Antenna Design and Applications at the European Conference in Antennas and Propagation (EuCAP) in April 2018 and also in the same year in August he won first place in the Student Paper Competition at the International Symposium on Antenna Technology and Applied Electromagnetics (ANTHEM) in Waterloo, Canada. In 2019, he was awarded the European Microwave Association Internship Award leading to a research placement with TNO Research and Defence in Netherlands, which was completed successfully in September 2020. He is a member of the IEEE Antennas and Propagation Society (AP-S), the IEEE Microwave Theory and Technology Society (MTT-S), and the IEEE Electron Devices Society. He is also the Secretary of the IEEE AP-S and MTT-S Joint Scottish Chapter, which won the Best Chapter in 2021 by MTT-S.

SYMON K. PODILCHAK (Member, IEEE) received the B.A.Sc. degree in engineering science from the University of Toronto, Toronto, ON, Canada, in 2005, and the M.A.Sc. and Ph.D. degrees in electrical engineering from Queen's University, Kingston, ON, Canada, in 2008 and 2013, respectively. From 2013 to 2015, he was an Assistant Professor with Queen's University. In 2015, he joined Heriot-Watt University, Edinburgh, U.K., as an Assistant Professor, and became an Associate Professor in 2017. He is currently a Senior Lecturer with the School of Engineering, The University of Edinburgh, Edinburgh, U.K. His research interests include surface waves, leaky-wave antennas, metasurfaces, UWB antennas, phased arrays, and RF integrated circuits. He has had industrial experience as a computer programmer, and has designed 24 and 77 GHz automotive radar systems with Samsung and Magna Electronics. His recent industry experiences also include the design of high frequency surface-wave radar systems, professional software design and implementation for measurements in anechoic chambers for the Canadian Department of National Defence and the SLOWPOKE Nuclear Reactor Facility. He has also designed compact antennas for wideband military communications, highly compact circularly polarized antennas for CubeSats with COM DEV International and The European Space Agency, and new wireless power transmission systems for Samsung.

Dr. Podilchak and his students were the recipient of many best paper awards and scholarships, most notably research fellowships from the IEEE Antennas and Propagation Society (AP-S), the IEEE Microwave Theory and Technology Society (MTT-S), the European Microwave Association, and six young scientist awards from the International Union of Radio Science. He was the recipient of the Postgraduate Fellowship from the Natural Sciences and Engineering Research Council of Canada (NSERC). In 2011, 2013, 2020, and 2021, he and his students received student paper awards at the IEEE International Symposium on Antennas and Propagation; in 2012, the Best Paper Prize for Antenna Design at the European Conference on Antennas and Propagation for his work on CubeSat antennas; and in 2016, the European Microwave Prize for his research on surface waves and leaky-wave antennas. In 2017 and 2019, he was bestowed a Visiting Professorship Award at Sapienza University, Rome, Italy, and from 2016 to 2019, his research was supported by a H2020 Marie Skłodowska-Curie European Research Fellowship. He was recognized as an outstanding reviewer of IEEE TRANSACTIONS ON ANTENNAS AND PROPAGATION, in 2014 and 2020. In 2021, he was the recipient of the COVID-19 Above and Beyond Medal for leading research on remote microwave sterilization of the coronavirus. He was also the Founder and First Chairman of the IEEE AP-S and IEEE MTT-S Joint Chapters in Canada and Scotland, in 2014 and 2019, respectively. In recognition of these services, he was presented with an Outstanding Volunteer Award from IEEE in 2015; and in 2020 and 2021, MTT-S and AP-S, respectively, recognized this Scotland Chapter for its activities and it was awarded the winner of the Outstanding Chapter Awards hosted by these two IEEE societies. He was also the recipient of the Outstanding Dissertation Award for his Ph.D. He was a Lecturer with the European School of Antennas and an Associate Editor for *IET Electronic Letters* and IEEE ANTENNAS AND WIRELESS PROPAGATION LETTERS. He is currently a Guest Associate Editor of IEEE OPEN JOURNAL OF ANTENNAS AND PROPAGATION. He is also a Registered Professional Engineer (P.Eng.).

PASCUAL D. HILARIO RE was born in Murcia, Spain. He received the B.Eng. and M.Sc. degrees in telecommunications engineering from the Universidad Politcnica de Cartagena, Cartagena, Spain, in 2012 and 2015, respectively, and the Ph.D. degree from Heriot-Watt University, Edinburgh, U.K., in 2019. His research interests include retro-directive systems, wireless power transmission applications, automotive radar, and analysis and design of power amplifiers.

THOMAS M. STRÖBER was born in Oberndorf bei Salzburg, Austria, in 1993. He received the M.Sc. degree in electrical and computer engineering from the Technical University of Munich, Munich, Germany, in 2017, and the Ph.D. degree in electrical engineering from the University of Rennes 1, Rennes, France, and Heriot-Watt University, Edinburgh, U.K., in 2020. His Ph.D. research was a part of the doctorate program RE-VOLVE under the European Commission's H2020 Marie Skłodowska-Curie Actions and carried out in part at the Research and Technologies Department, Thales Alenia Space, Toulouse, France. His research interests include the analysis and design of quasi-optical beamformers, asymptotic high-frequency methods, gap waveguide technology, and conformal metasurfaces.

YAN PAILHAS received the two Engineering degrees in telecommunications with a specialization in image and signal processing from the Ecole Nationale Superieure des Telecommunications, Paris, France, and the Politecnico di Torino, Torino, Italy, the M.Sc. degree in signal and image processing from the Ecole Nationale Superieure de Cachan, Cachan, France, in 2003, and the Ph.D. degree in sonar systems and underwater acoustics from Heriot-Watt University, Edinburgh, U.K., in 2012. Since 2004, he has been a Research Associate with Ocean Systems Laboratory, Heriot-Watt University, where he is currently carrying out research activities in bioacoustic signals and sensors, signal processing for detection and classification, and numerical simulations.

CAROLINA MATEO-SEGURA was born in Valencia, Spain, in 1981. She received the M.Sc. degree in telecommunications engineering from the Polytechnic University of Valencia, Valencia, Spain, in 2006, and the joint Ph.D. degree from the University of Edinburgh, Edinburgh, U.K., and Heriot-Watt University, Edinburgh, U.K., in 2010. In 2006, she joined the Department of Security and Defence, Indra Systems, Madrid, Spain, as a Junior Engineer. In 2009, she was a Research Associate with the Wireless Communications Research Group, Loughborough University, Loughborough, U.K. In December 2010, she joined the Antennas and Electromagnetics Research Group, Queen Mary University of London, London, U.K., as a Research Associate, where she worked on the electromagnetic modeling and design of novel metamaterial antennas for high-power applications. Her research interests include the analysis and design of frequency selective surfaces, artificial periodic electromagnetic structures with applications on high-gain array antennas and medical imaging systems, transformation electromagnetics, and numerical techniques for electromagnetics.

MATHINI SELLATHURAI (Senior Member, IEEE) is currently a Professor of signal processing and wireless communications and the Dean of Science and Engineering with Heriot-Watt University, Edinburgh, U.K. She has been active in signal processing research for the past 20 years and has a strong international track record in multiple-input, multiple-output signal processing with applications in radar, and wireless communications. She held visiting positions with Bell-Laboratories, Holmdel, NJ, USA, and with The Canadian Communications Research Centre, Ottawa, ON, Canada. She has authored or coauthored more than 200 peer-reviewed papers in leading international journals and IEEE conferences, given invited talks and has written several book chapters and a research monograph as a lead author. Her research interests include full-duplex systems, passive radar topography, localisation, massive-MIMO, non-orthogonal multiple access, waveform designs, caching technologies, assisted care technologies, IoT, hearing-aids, optimal coded-modulation designs using auto-encoders, channel prediction, and mm-wave imaging and communications.

Dr. Sellathurai was the recipient of the IEEE Communication Society Fred W. Ellersick Best Paper Award in 2005, Industry Canada Public Service Awards for contributions to Science and Technology in 2005, and awards for contributions to Technology Transfers to Industry in 2004. She was the recipient of the Natural Sciences and Engineering Research Council of Canada Doctoral Award for her Ph.D. dissertation in 2002. She was the Editor of IEEE TRANSACTIONS ON SIGNAL PROCESSING from 2009 to 2014 and 2015 to 2018, the General Co-Chair of IEEE SPAWC2016 in Edinburgh, and a member of the IEEE SPCOM Technical Strategy Committee from 2014 to 2019.

GEORGE GOUSSETIS (Senior Member, IEEE) received the Diploma in electrical and computer engineering from the National Technical University of Athens, Athens, Greece, in 1998, the B.Sc. degree in physics (Hons.) from University College London, London, U.K., in 2002, and the Ph.D. degree from the University of Westminster, London, U.K., in 2002. In 1998, he joined Space Engineering, Rome, Italy, as an RF Engineer, and in 1999, he was a Research Assistant with Wireless Communications Research Group, University of Westminster, London, U.K. From 2002 to 2006, he was a Senior Research Fellow with Loughborough University, Loughborough, U.K. From 2006 to 2009, he was a Lecturer (Assistant Professor) with Heriot-Watt University, Edinburgh, U.K., and a Reader (Associate Professor) with Queen's University Belfast, Belfast, U.K., from 2009 to 2013. In 2013, he joined Heriot-Watt, as a Reader, and was promoted to a Professor in 2014. He has authored or coauthored more than 200 peer-reviewed papers, five book chapters, one book, and two patents. His research interests include the modeling and design of microwave filters, frequency-selective surfaces and periodic structures, leaky wave antennas, microwave sensing, and curing as well numerical techniques for electromagnetics. He has held a research fellowship with the Onassis Foundation in 2001, a Research Fellowship with the U.K. Royal Academy of Engineering from 2006 to 2011, and a European Marie-Curie Experienced Researcher Fellowship from 2011 to 2012.

Mr. Goussetis was a co-recipient of the 2011 European Space Agency Young Engineer of the Year Prize, the 2011 EuCAP Best Student Paper Prize, the 2012 EuCAP Best Antenna Theory Paper Prize, and the 2016 Bell Labs Prize.

YVAN R. PETILLOT received the Engineering degree in telecommunications with a specialization in image and signal processing, the M.Sc. degree in optics and signal processing, and the Ph.D. degree in real-time pattern recognition using optical processors from the Ecole Nationale Supérieure des Télécommunications de Bretagne, Universitée de Bretagne Occidentale, Brest, France. He is a specialist of sonar data processing (including obstacle avoidance) and sensor fusion. He is currently a Professor with the University of Heriot-Watt, Edinburgh, U.K., where he leads the Sensor Processing Group, Oceans Systems Laboratory. His research interests include image interpretation and mine and counter measures.

Dr. Petillot is a reviewer of various IEEE transactions.

JOHN S. THOMPSON (Fellow, IEEE) received the Ph.D. degree in electrical engineering from the University of Edinburgh, Edinburgh, U.K., in 1995. He is currently a Professor with the School of Engineering, University of Edinburgh. He has authored or coauthored more than 350 papers on the topics of his research interests, which include antenna array processing, cooperative communications systems, energy efficient wireless communications, and their applications.

Dr. Thompson was the Co-Chair of the IEEE International Conference on Communications, Control, and Computing Technologies for Smart Grids (SmartGridComm) held in Aalborg, Denmark. He currently participates in two U.K. research projects, which study new concepts for signal processing and next-generation wireless communications. In January 2016, he was elevated to Fellow of IEEE for contributions to antenna arrays and multihop communications. During 2015–2018, he was recognized by Thomson Reuters as a highly cited researcher.

JAESUP LEE received the M.S. degree in electrical engineering from the University of California at Los Angeles, Los Angeles, CA, USA. He is currently with the Samsung Advanced Institute of Technology, Suwon, South Korea. His research interests include RF and analog circuits, especially ultra-low-power personal network platforms, RF wireless power transfer, and radar.